A bi-projection method for Bingham type flows

Laurent Chupin, Thierry Dubois

A BI-PROJECTION METHOD FOR BINGHAM TYPE FLOWS

LAURENT CHUPIN, THIERRY DUBOIS

Abstract. We propose and study a new numerical scheme to compute the isothermal and unsteady flow of an incompressible viscoplastic Bingham medium. The main difficulty, for both theoretical and numerical approaches, is due to a lack of definition of the plastic stress tensor in aeras where the deformation tensor vanishes. This is handled by introducing a projection formulation for the yield stress tensor. A new time scheme based on the classical incremental projection method for the Newtonian Navier-Stokes equations is proposed. The plastic tensor is treated implicitely in the first sub-step of the projection scheme and is computed by using a fixed point procedure, which is shown to converge geometrically. This key feature of our method ensures its numerical efficiency. Stability and error analyses of the numerical scheme are provided. A first-order estimate of the time error is obtained for the velocity field. A second-order cell-centered finite volume scheme on a staggered grid is applied for the spatial discretization. The scheme is assessed against previous plubished benchmark results for both Newtonian and Bingham flows in a lid-driven cavity at Reynolds number equals 10^3. The proposed numerical scheme is able to reproduce the fundamental property of cessation in finite time of a viscoplastic medium in the absence of any energy source term in the equations.

1. Introduction

Many materials occuring in industrial or geophysical problems, such as pastes or polymer suspensions, muds used in drilling technologies, lavas, even blood in arterioles and capilliries, behave as viscous fluid flows in regions of high shear stress and as rigid bodies where the stress is below a critical value, called the yield stress. A typical situation found in engineering context is the solidification of flows of a viscoplastic medium in pipes. An important property of flows of non-newtonian materials, called Bingham fluids, is that the velocity fields goes to zero (the flow halts) in a finite time in the absence of any energy source terms. The model which takes into account such viscoplastic behavior is known as the Bingham model and corresponds to the momentuum conservation law for which the stress has a singularity (corresponding to the yield stress). More precisely, when the shear strain rate magnitude vanishes, the shear stress is not defined.

This singularity is a permanent source of challenging problems both from the theoretical point of view and in the design of efficient numerical algorithms capable to produce reliable and accurate numerical simulations. In order to handle this non-differentiability of the constituve rheological law, two approaches have been mainly used both in the fields of theoretical studies and numerical simulations. The first one consists in approximating the Bingham model by a *smooth* (differentiable) functionnal, see for instance [3] and [20]. Such regularizing methods are appealing as they can be easily incorporated in classical numerical schemes and implemented in many existing codes designed for the numerical simulation of flows of newtonian viscous fluids.

Date: June 23, 2015.

Key words and phrases. Bingham fluids; Unsteady flows; Incremental projection scheme; Finite volume; Staggered mesh; Lid-driven cavity; Parallel computing.

They have been widely used to perform numerical simulations of flows of an incompressible Bingham medium, see for instance [3], [15] and [5]. As it is mentioned in [5], regularization methods do not accurately reproduce the cessation of Bingham fluid flows in finite time. Let us mention that Zhang in [27] performed a numerical analysis of a regularized Bingham model [3] and derived both time and spatial error bounds for a fully discrete system of equations.

The second approach, used to overcome the difficulty due to the non-differentiable form of the constitutive law, relies on the theory of variational inequalities due to Duvaut and Lions [9]. In this context the Bingham equations can be interpreted with Lagrange multipliers so that the problem reduces in solving several saddle-point problems. These minimisation problems are generally solved by using the Augmented Lagrangian method [10] or the Uzawa-like method [11]. A review of numerical schemes based on this approach can be found in [7]. The variational inequality formulation is particularly well suited for finite element approximations. Therefore, these methods have been mostly used in the context of finite element method for the spatial discretization of the equations [7, 26, 21]. Numerical schemes based on the finite difference method to discretize the spatial partial derivatives have been more recently proposed and used. Two type of schemes have been employed whose main differences rely in the choice of the locations of the dicrete variables on the computational grid, namely staggered in [17, 16] and semi-staggered in [19, 18].

Regarding the time discretization of the (non-regularized) Bingham problem, operator splitting methods are commonly used (see [22, 6, 26]). Most contributions in this context use three sub-steps for the computation of the velocity field over one time step. They decouple the resolution of the Stokes operator, that is the viscous term including the incompressibility constraint, the nonlinear (transport) terms and the (plastic) Bingham contribution. Obviously, the main advantage of this type of scheme is to separate and isolate the difficulties so that efficient and well-known numerical schemes can be applied for solving each sub-steps.

Projection methods are widely used for the time discretization of the incompressible Navier-stokes equations [12] especially in the context of the numerical simulation of turbulent flows. Indeed, coupling a projection scheme with a cell-centered finite difference/volume scheme for the nonlinear (advection) terms on a staggered grid allows to recover at the discrete level the fundamental orthogonality property (with respect to the L^2-inner product and its discrete counterpart) of the nonlinear terms with the velocity field. This ensures conservation of the kinetic energy for an inviscid flow. Surprisingly, projection schemes have not been used in the numerical studies of Bingham viscoplastic flows until recently. Indeed, Muravleva in [16] proposed a three-level splitting scheme consisting of a second-order (BDF2) projection scheme for the first two steps followed by a plasticity step computing the plastic stress tensor.

In this paper, we introduce a new time discretization scheme to solve the non-regularized Bingham problem. The main idea is to couple an incremental projection scheme with a projection, of the Uzawa-like method type (see [7, 16]), to treat the Bingham singularity. Unlike in [16], the plastic stress tensor is added implicitely in the prediction step of the projection scheme and is computed as the fixed point of a projection operator. The Bingham projection is solved with a fixed point procedure which is shown to convergence geometrically. This ensures the computational efficiency of the proposed scheme. The objective of this paper is first to perform a numerical analysis (stability study and error analysis) of our bi-projection scheme and to show the efficiency of the proposed new methodologies by performing numerical simulations on classical and well-known computational configurations.

The outline of the rest of the paper is as follows. In section 2 we precisely provide the mathematical formulation, and the notations, for a Bingham (non-regularized) viscoplastic model. We also introduce the projection formulation, used to compute the extra (plastic) stress tensor, which will be used in the next parts. In section 3 we introduce an iterative method (with respect to the time) in order to approximate the continuous model. In this section, we prove that this method is well posed, stable and converging. In the last section 4, we first describe in details the spatial and time discretization scheme used for the numerical simulations. Finally, some numerical experiments, highlighting the efficiency of the proposed new methodologies, are performed and analyzed.

2. The model of a Bingham viscous plastic flow

2.1. **Mathematical modelling.** Let $T > 0$ be a positive real number and Ω be a domain of $\mathbb{R}^d$. The isothermal flow of an incompressible Bingham viscoplastic medium is modeled by the following system of equations on the velocity $\mathbf{u}$ and the pressure p:

$$\begin{cases} \rho_0\big(\partial_t \mathbf{u} + \mathbf{u}\cdot\nabla\mathbf{u}\big) + \nabla p = \operatorname{div}\boldsymbol{\tau} & \text{in } (0,T)\times\Omega, \\ \operatorname{div}\mathbf{u} = 0 & \text{in } (0,T)\times\Omega, \end{cases} \tag{1}$$

where the stress $\boldsymbol{\tau}$ is given with respect to the deformation tensor $\mathrm{D}\mathbf{u}$ by the relation

$$\boldsymbol{\tau} = 2\mu_0\,\mathrm{D}\mathbf{u} + \sigma_0\frac{\mathrm{D}\mathbf{u}}{|\mathrm{D}\mathbf{u}|}. \tag{2}$$

In this system (1)–(2), the constant ρ_0 represents the density of the medium, the constant μ_0 corresponds to its viscosity and the constant σ_0 is the plasticity yield[1]. The tensor $\mathrm{D}\mathbf{u}$ represents the deformation tensor, *i.e.* the symmetric part of the velocity gradient, and $|\mathrm{D}\mathbf{u}|$ is its Froebenius norm:

$$\mathrm{D}\mathbf{u} = \frac{1}{2}\big(\nabla\mathbf{u} + {}^T(\nabla\mathbf{u})\big) \qquad \text{and} \qquad |\mathrm{D}\mathbf{u}|^2 = \sum_{1\le i,j\le d} |(\mathrm{D}\mathbf{u})_{ij}|^2.$$

Finally the system is closed given an initial condition ($\mathbf{u} = \mathbf{u}_0$ for $t = 0$) and boundary conditions ($\mathbf{u} = \mathbf{u}_b$ on $\partial\Omega$). For the sake of simplicity and only for the theoretical analysis of the numerical scheme, we shall consider only homogeneous Dirichlet boundary conditions, namely: $\mathbf{u}_b = \mathbf{0}$. We point out that some of our results remain true for the case of nonhomogeneous boundary conditions when $\mathbf{u}_b$ is tangent to the boundary.

We observe that (if $\sigma_0 > 0$) the above model makes no sense on the rigid set, that is where the deformation tensor $\mathrm{D}\mathbf{u}$ vanishes. Indeed the equation (2) must read

$$\boldsymbol{\tau} = 2\mu_0\,\mathrm{D}\mathbf{u} + \sigma_0\,\boldsymbol{\sigma},$$

where the extra-stress tensor $\boldsymbol{\sigma}$ satisfies

$$\begin{cases} \boldsymbol{\sigma} = \dfrac{\mathrm{D}\mathbf{u}}{|\mathrm{D}\mathbf{u}|} & \text{if } |\mathrm{D}\mathbf{u}| \neq 0, \\ |\boldsymbol{\sigma}| \le 1 & \text{if } |\mathrm{D}\mathbf{u}| = 0. \end{cases} \tag{3}$$

Consequently the stress contribution $\boldsymbol{\sigma}$ is not always well-defined.

[1]Note that in some papers (for instance [7]), the plasticity yield is $\sqrt{2}\,\sigma_0$.

2.2. **The projection formulation.** In order to avoid this problem of non-well-definition of the stress $\boldsymbol{\sigma}$, several methods are possible. We chose a method of projection type, as defined in the following proposition.

Proposition 1. *For all $r > 0$ the condition* (3) *is equivalent to the relation*

$$\boldsymbol{\sigma} = \mathbb{P}(\boldsymbol{\sigma} + r\,\mathrm{D}\mathbf{u}), \tag{4}$$

where $\mathbb{P}$ is the projector on the closed convex set defined by

$$\Lambda := \Big\{ \boldsymbol{\sigma} \in L^2(\Omega)^{d\times d} \quad ; \quad |\boldsymbol{\sigma}(\mathbf{x})| \leq 1 \ \textit{a.e. on}\ \Omega \Big\}.$$

Proof. If $|\mathrm{D}\mathbf{u}| = 0$ the equivalence is obvious: we have $\boldsymbol{\sigma} \in \Lambda$.
We now assume that $|\mathrm{D}\mathbf{u}| \neq 0$. Note that an explicit expression of the projection $\mathbb{P}$ is given by (almost everywhere on Ω):

$$\mathbb{P}(\boldsymbol{\sigma}) = \begin{cases} \boldsymbol{\sigma} & \text{if } |\boldsymbol{\sigma}| \leq 1, \\ \boldsymbol{\sigma}/|\boldsymbol{\sigma}| & \text{if } |\boldsymbol{\sigma}| > 1. \end{cases} \tag{5}$$

Consequently if $\boldsymbol{\sigma} = \dfrac{\mathrm{D}\mathbf{u}}{|\mathrm{D}\mathbf{u}|}$ then $\boldsymbol{\sigma} + r\,\mathrm{D}\mathbf{u} = (1 + r|\mathrm{D}\mathbf{u}|)\dfrac{\mathrm{D}\mathbf{u}}{|\mathrm{D}\mathbf{u}|}$ satisfies the equality

$$\mathbb{P}(\boldsymbol{\sigma} + r\,\mathrm{D}\mathbf{u}) = \frac{\mathrm{D}\mathbf{u}}{|\mathrm{D}\mathbf{u}|},$$

so that $\mathbb{P}(\boldsymbol{\sigma} + r\,\mathrm{D}\mathbf{u}) = \boldsymbol{\sigma}$.
Reciprocally, if $\boldsymbol{\sigma} = \mathbb{P}(\boldsymbol{\sigma} + r\,\mathrm{D}\mathbf{u})$ then $|\boldsymbol{\sigma} + r\,\mathrm{D}\mathbf{u}| > 1$ (otherwise, using (5) we would have $\mathrm{D}\mathbf{u} = \mathbf{0}$) and we have

$$\boldsymbol{\sigma} = \frac{\boldsymbol{\sigma} + r\,\mathrm{D}\mathbf{u}}{|\boldsymbol{\sigma} + r\,\mathrm{D}\mathbf{u}|}.$$

In particular we have $|\boldsymbol{\sigma}| = 1$ and

$$\boldsymbol{\sigma} = \frac{r}{|\boldsymbol{\sigma} + r\,\mathrm{D}\mathbf{u}| - 1}\mathrm{D}\mathbf{u}.$$

We then deduce that $\boldsymbol{\sigma} = \dfrac{\mathrm{D}\mathbf{u}}{|\mathrm{D}\mathbf{u}|}$. □

Remark 1.

✓ *The most usual method to solve the Bingham problem* (1)–(2) *is to rewrite the condition* (3) *using a variational inequality model (see* [9]*). This method has been widely used (both theoretically and numerically) and is suitable for numerical schemes of finite volume type since it is written using integral formulation.*

✓ *Another idea is to introduce a small parameter ϵ and to reguralize* (2) *by writing*

$$\boldsymbol{\tau} = 2\mu_0\,\mathrm{D}\mathbf{u} + \sigma_0\frac{\mathrm{D}\mathbf{u}}{|\mathrm{D}\mathbf{u}| + \varepsilon}.$$

This approach has many advantages from a theoretical point of view. One can relatively easily show the existence of a solution $(\mathbf{u}_\varepsilon, p_\varepsilon)$ for each value of ε. Passing to the limit $\varepsilon \to 0$, the existence of a solution $(\mathbf{u}, p)$ to the original problem (1)–(2) *can be obtained. Nevertheless, from a numerical point of view the behavior of $(\mathbf{u}_\varepsilon, p_\varepsilon)$, even for small values of ε, can be quite different from the desired behavior. For instance, without source term (that is without external volume force as in* (1) *and with $\mathbf{u}_b = \mathbf{0}$) the well-known property that $\mathbf{u}(t) \to 0$ in finite time is lost.*

2.3. **Dimensionless Bingham system.** In order to write the system in dimensionless form we introduce a characteristic length L and a characteristic velocity V. Consequently, the natural characteristic time is given by L/V, a characteristic pressure by $\rho_0 V^2$ and a characteristic stress by σ_0. We denote the Reynolds number and the Bingham number by

$$\mathfrak{R}e = \frac{\rho_0 V L}{\mu_0} \quad \text{and} \quad \mathfrak{B}i = \frac{\sigma_0 L}{\mu_0 V},$$

so that the model of a Bingham viscous plastic flow (1)–(2) reads in dimensionless form:

$$\partial_t \mathbf{u} + \mathbf{u}\cdot\nabla\mathbf{u} + \nabla p - \frac{1}{\mathfrak{R}e}\Delta\mathbf{u} = \frac{\mathfrak{B}i}{\mathfrak{R}e}\,\mathrm{div}\,\boldsymbol{\sigma}, \tag{6}$$

under the two conditions (r being any positive parameter)

$$\mathrm{div}\,\mathbf{u} = 0 \qquad \text{and} \qquad \boldsymbol{\sigma} = \mathbb{P}(\boldsymbol{\sigma} + r\,\mathrm{D}\mathbf{u}). \tag{7}$$

3. Theoretical results on a simple scheme

3.1. **Time discretization.** In this section, we propose a new scheme to discretise with respect to the time variable the Stokes-Bingham equations, that is the previous equations (6)–(7) without taking into account the convective term $\mathbf{u}\cdot\nabla\mathbf{u}$:

$$\begin{cases} \partial_t \mathbf{u} + \nabla p - \dfrac{1}{\mathfrak{R}e}\Delta\mathbf{u} = \dfrac{\mathfrak{B}i}{\mathfrak{R}e}\,\mathrm{div}\,\boldsymbol{\sigma}, \\ \mathrm{div}\,\mathbf{u} = 0, \\ \boldsymbol{\sigma} = \mathbb{P}(\boldsymbol{\sigma} + r\,\mathrm{D}\mathbf{u}). \end{cases} \tag{8}$$

Remark 2. *In practice, the nonlinear term $\mathbf{u}\cdot\nabla\mathbf{u}$, which can be rewritten as $div(\mathbf{u}\otimes\mathbf{u})$ due to the incompressibility constraint, will be taken into account when performing numerical simulations (see the section 4). However, in order to avoid unnecessary technical difficulties, we present hereafter a convergence and error analysis only in the linear (Stokes) case. Indeed, the essential difficulty here comes from the coupling between a projection scheme for the Stokes operator with the projection* (4) *of the yield stress tensor.*

In order to solve (8) we advocate the fixed point algorithm below in which we introduce four numerical parameters (δt, r, α and θ):

We start with $\mathbf{u}^0 = \mathbf{u}_0$ and with arbitrary $\boldsymbol{\sigma}^0$ and p^0.

For $n \geq 0$, assuming that $\mathbf{u}^n$, $\boldsymbol{\sigma}^n$ and p^n is known, we compute $(\widetilde{\mathbf{u}}^{n+1}, \boldsymbol{\sigma}^{n+1})$ as the solution of

$$\begin{cases} \dfrac{\widetilde{\mathbf{u}}^{n+1} - \mathbf{u}^n}{\delta t} + \nabla p^n - \dfrac{1}{\mathfrak{R}e}\Delta\widetilde{\mathbf{u}}^{n+1} = \dfrac{\mathfrak{B}i}{\mathfrak{R}e}\,\mathrm{div}\,\boldsymbol{\sigma}^{n+1}, \\ \boldsymbol{\sigma}^{n+1} = \mathbb{P}(\boldsymbol{\sigma}^{n+1} + r\,\mathrm{D}\widetilde{\mathbf{u}}^{n+1} + \theta(\boldsymbol{\sigma}^n - \boldsymbol{\sigma}^{n+1})), \\ \widetilde{\mathbf{u}}^{n+1}\Big|_{\partial\Omega} = \mathbf{0}. \end{cases} \tag{9}$$

Next, we deduce $(\mathbf{u}^{n+1}, p^{n+1})$ using the free-divergence constraint:

$$\begin{cases} \dfrac{\mathbf{u}^{n+1} - \widetilde{\mathbf{u}}^{n+1}}{\delta t} + \alpha\nabla(p^{n+1} - p^n) = \mathbf{0}, \\ \mathrm{div}\,\mathbf{u}^{n+1} = 0, \\ \mathbf{u}^{n+1}\cdot\mathbf{n}\Big|_{\partial\Omega} = 0. \end{cases} \tag{10}$$

We will prove in the next section that the sequence $(\mathbf{u}^n)_n$ converges to the solution $\mathbf{u}$ of the system (8), see Theorem 3.
In practice, to solve the ystem (9) we use the following sub-fixed-point:

$$\mathbf{u}^n, \quad \boldsymbol{\sigma}^{n,0} = \boldsymbol{\sigma}^n \quad \text{and} \quad p^n \quad \text{given.}$$

For $k \geq 0$, assuming that $\boldsymbol{\sigma}^{n,k}$ is known, we first compute $\widetilde{\mathbf{u}}^{n,k}$ as the solution of a Laplace type problem and then we project the stress tensor to deduce $\boldsymbol{\sigma}^{n,k+1}$:

$$\left\{ \begin{array}{l} \dfrac{\widetilde{\mathbf{u}}^{n,k} - \mathbf{u}^n}{\delta t} + \nabla p^n - \dfrac{1}{\mathfrak{R}e} \Delta \widetilde{\mathbf{u}}^{n,k} = \dfrac{\mathfrak{B}i}{\mathfrak{R}e} \operatorname{div} \boldsymbol{\sigma}^{n,k}, \\ \widetilde{\mathbf{u}}^{n,k}\Big|_{\partial\Omega} = \mathbf{0}, \\ \boldsymbol{\sigma}^{n,k+1} = \mathbb{P}(\boldsymbol{\sigma}^{n,k} + r\, \mathrm{D}\widetilde{\mathbf{u}}^{n,k} + \theta(\boldsymbol{\sigma}^n - \boldsymbol{\sigma}^{n,k})). \end{array} \right. \tag{11}$$

We will prove in the next section that the sequence $(\widetilde{\mathbf{u}}^{n,k}, \boldsymbol{\sigma}^{n,k})_k$ obtained converges to the solution $(\widetilde{\mathbf{u}}^{n+1}, \boldsymbol{\sigma}^{n+1})$ of the system (9), see Theorem 1.

3.2. **Notations.** The equations introduced before depend on parameters. Some physical parameters like $\mathfrak{R}e$ and $\mathfrak{B}i$, and some numerical parameters: r, θ, α and δt. All these parameters are always supposed to be positive.

For two vectors $\mathbf{u}$, $\mathbf{v}$ in $\mathbb{R}^d$, we denote by $\mathbf{u} \cdot \mathbf{v}$ the inner product:

$$\mathbf{u} \cdot \mathbf{v} = \sum_{i=1}^{d} u_i\, v_i.$$

For two tensors $\boldsymbol{\sigma}$, $\boldsymbol{\tau}$ in $\mathbb{R}^{d\times d}$, we denote by $\boldsymbol{\sigma} : \boldsymbol{\tau}$ the inner product:

$$\boldsymbol{\sigma} : \boldsymbol{\tau} = \sum_{1\leq i,j\leq d} \sigma_{ij}\, \tau_{ij}.$$

In both cases, the associated norm will be denoted $|\cdot|$.

For two functions f, g defined on the open set $\Omega \subset \mathbb{R}^d$ with values in $\mathbb{R}$, we will use the notation $\langle f, g\rangle$ for the inner product in $L^2(\Omega)$:

$$\langle f, g\rangle = \int_\Omega f\, g.$$

The associated $L^2(\Omega)$-norm will be denoted $\|\cdot\|_{L^2(\Omega)}$. For the sake of simplicity, the same notations for the inner product and the norm will be used throughout this paper for functions with values in $\mathbb{R}^d$ and $\mathbb{R}^{d\times d}$.

In some cases, we use other functional spaces norms. These are always indicated in index, for example $\|f\|_{H^{-1}(\Omega)}$ for the norm associated to the Sobolev space $H^{-1}(\Omega)$.

Let N be an integer and $\{t_n\}_{n\in\{0,\dots,N\}}$ be a family of discretization of $[0,T]$. For simplicity, we use a uniform discretization so that:

$$t_n = n\,\delta t \qquad \text{with} \quad \delta t = \frac{T}{N}.$$

3.3. **Well-posedness.** At first we indicate that each problem previously introduced is well-posed.

✓ It is well known that the Stokes-Bingham system (8) has a solution $(\mathbf{u}, p, \boldsymbol{\sigma})$, see for instance [9] where the variational inequality formulation is used. The uniqueness is clearly false since there exists many stress tensors $\boldsymbol{\sigma}$ on the set where $\mathrm{D}\mathbf{u} = \mathbf{0}$. Nevertheless, it can be proved that the velocity $\mathbf{u}$ is always well-defined, and the pressure p is well-defined too, up to an additive constant.

✓ The existence and uniqueness for the solution $(\widetilde{\mathbf{u}}^{n+1}, \boldsymbol{\sigma}^{n+1})$ to system (9) result from the theory of variational inequations too. The precise result for this system is proved in [7, p. 47].

✓ The system (10) is more usual: $\widetilde{\mathbf{u}}^{n+1}$ and p^n given, it admits a unique solution $(\mathbf{u}^{n+1}, p^{n+1})$, up to an additive constant for the pressure field. Indeed, $\mathbf{u}^{n+1} = \mathbb{P}_H \widetilde{\mathbf{u}}^{n+1}$ where $\mathbb{P}_H$ is the orthogonal projector in $L^2(\Omega)^d$ onto the free-divergence vector space, and the pressure p^{n+1} is a solution of the following Poisson equation

$$\Delta p^{n+1} = \Delta p^n + \frac{1}{\alpha\,\delta t}\,\mathrm{div}\,\widetilde{\mathbf{u}}^{n+1} \qquad \text{supplemented with} \qquad \frac{\partial (p^{n+1} - p^n)}{\partial \mathbf{n}}\Big|_{\partial\Omega} = 0.$$

✓ For each integer $n \in \mathbb{N}$, we show by induction on the integrer k that each couple $(\widetilde{\mathbf{u}}^{n,k}, \boldsymbol{\sigma}^{n,k})$ is well defined as the solution of system (11). In particular the existence and uniqueness of $\widetilde{\mathbf{u}}^{n,k}$ are ensured by the Lax-Milgram theorem.

3.4. **Convergence results with respect to k.**

Theorem 1. *We assume that*

$$2\theta + r\,\mathfrak{B}i \leq 2.$$

For each integer $n \in \mathbb{N}$, the sequence $(\widetilde{\mathbf{u}}^{n,k}, \boldsymbol{\sigma}^{n,k})_k$ solution of system (11) converges to $(\widetilde{\mathbf{u}}^{n+1}, \boldsymbol{\sigma}^{n+1})$, solution of system (9), as k tends to $+\infty$.
Moreover the convergence is geometric with common ratio $1 - \theta$.

Proof. Denoting $\overline{\mathbf{u}}^k = \widetilde{\mathbf{u}}^{n,k} - \widetilde{\mathbf{u}}^{n+1}$ and $\overline{\boldsymbol{\sigma}}^k = \boldsymbol{\sigma}^{n,k} - \boldsymbol{\sigma}^{n+1}$ we obtain by subtracting (9) from (11) that, for all $k \geq 0$,

$$\text{(12)} \qquad \begin{cases} \dfrac{1}{\delta t}\overline{\mathbf{u}}^k - \dfrac{1}{\mathfrak{R}e}\Delta\overline{\mathbf{u}}^k = \dfrac{\mathfrak{B}i}{\mathfrak{R}e}\,\mathrm{div}\,\overline{\boldsymbol{\sigma}}^k, \\ \overline{\mathbf{u}}^k\Big|_{\partial\Omega} = 0, \\ \overline{\boldsymbol{\sigma}}^{k+1} = \mathbb{P}(\boldsymbol{\sigma}^{n,k} + r\,\mathrm{D}\widetilde{\mathbf{u}}^{n,k} + \theta(\boldsymbol{\sigma}^n - \boldsymbol{\sigma}^{n,k})) \\ \qquad\qquad - \mathbb{P}(\boldsymbol{\sigma}^{n+1} + r\,\mathrm{D}\widetilde{\mathbf{u}}^{n+1} + \theta(\boldsymbol{\sigma}^n - \boldsymbol{\sigma}^{n+1})). \end{cases}$$

We now take the inner product of the first equation in (12) by $\overline{\mathbf{u}}^k$ in $L^2(\Omega)$ to deduce

$$\text{(13)} \qquad \frac{1}{\delta t}\|\overline{\mathbf{u}}^k\|^2_{L^2(\Omega)} + \frac{1}{\mathfrak{R}e}\|\nabla\overline{\mathbf{u}}^k\|^2_{L^2(\Omega)} = -\frac{\mathfrak{B}i}{\mathfrak{R}e}\langle\overline{\boldsymbol{\sigma}}^k, \mathrm{D}\overline{\mathbf{u}}^k\rangle.$$

Since $\mathbb{P}$ is a projection operator, the last equation in (12) implies

$$|\overline{\boldsymbol{\sigma}}^{k+1}| \leq |(1-\theta)\overline{\boldsymbol{\sigma}}^k + r\,\mathrm{D}\overline{\mathbf{u}}^k|.$$

Taking the $L^2(\Omega)$-norm, we deduce (using $|\mathrm{D}\overline{\mathbf{u}}^k| \leq |\nabla\overline{\mathbf{u}}^k|$) that

$$\begin{aligned}\|\overline{\boldsymbol{\sigma}}^{k+1}\|_{L^2(\Omega)}^2 \leq (1-\theta)^2\|\overline{\boldsymbol{\sigma}}^k\|_{L^2(\Omega)}^2 + r^2\|\nabla\overline{\mathbf{u}}^k\|_{L^2(\Omega)}^2 \\ + 2r(1-\theta)\langle\overline{\boldsymbol{\sigma}}^k, \mathrm{D}\overline{\mathbf{u}}^k\rangle.\end{aligned} \tag{14}$$

Combining the equality (13) and the inequality (14) we obtain

$$\begin{aligned}&\frac{\mathfrak{B}i}{\mathfrak{R}e}\|\overline{\boldsymbol{\sigma}}^{k+1}\|_{L^2(\Omega)}^2 + \frac{2r(1-\theta)}{\delta t}\|\overline{\mathbf{u}}^k\|_{L^2(\Omega)}^2 \\ &\quad + \frac{r(2-2\theta-r\,\mathfrak{B}i)}{\mathfrak{R}e}\|\nabla\overline{\mathbf{u}}^k\|_{L^2(\Omega)}^2 \leq \frac{\mathfrak{B}i}{\mathfrak{R}e}(1-\theta)^2\|\overline{\boldsymbol{\sigma}}^k\|_{L^2(\Omega)}^2.\end{aligned} \tag{15}$$

We then deduce that, if $2\theta + r\mathfrak{B}i \leq 2$ all the coefficients in the left-hand side of the inequality (15) are positive. Therefore, we have

$$\begin{aligned}&\|\overline{\boldsymbol{\sigma}}^k\|_{L^2(\Omega)} \leq (1-\theta)^k\|\overline{\boldsymbol{\sigma}}^0\|_{L^2(\Omega)}, \\ &\|\overline{\mathbf{u}}^k\|_{L^2(\Omega)} \leq \sqrt{\frac{\mathfrak{B}i\,\delta t\,(1-\theta)}{2r\,\mathfrak{R}e}}(1-\theta)^k\|\overline{\boldsymbol{\sigma}}^0\|_{L^2(\Omega)}, \\ &\|\nabla\overline{\mathbf{u}}^k\|_{L^2(\Omega)}^2 \leq \sqrt{\frac{\mathfrak{B}i}{r(2-2\theta-r\,\mathfrak{B}i)}}(1-\theta)^k\|\overline{\boldsymbol{\sigma}}^0\|_{L^2(\Omega)},\end{aligned}$$

which concludes the proof of Theorem 1. □

3.5. **Stability result with respect to n.**

Theorem 2 (Stability)**.** *We assume that*

$$\alpha \geq 1, \qquad r\,\mathfrak{B}i \leq 1 \quad \textit{and} \quad \theta \leq 1/2.$$

The sequence $(\mathbf{u}^n, \widetilde{\mathbf{u}}^n, p^n, \boldsymbol{\sigma}^n)_n$ solution of the system (9)–(10) is bounded.

We note that the assumptions of Theorem 2 implies that the assumption also holds for Theorem 1.

Proof. By definition of the sequence $(\boldsymbol{\sigma}_n)_n$ and the projection $\mathbb{P}$, it is obvious that $\boldsymbol{\sigma}_n$ is bounded by unity. The method consists in deriving an estimate on the velocity sequence, and on the pressure sequence. We first take the inner product of the first equation of (9) with $2\delta t\,\widetilde{\mathbf{u}}^{n+1}$ in $L^2(\Omega)^d$; using the identity

$$2a(a-b) = a^2 - b^2 + (a-b)^2, \tag{16}$$

we derive

$$\begin{aligned}\|\widetilde{\mathbf{u}}^{n+1}\|_{L^2(\Omega)}^2 - \|\mathbf{u}^n\|_{L^2(\Omega)}^2 + \|\widetilde{\mathbf{u}}^{n+1} - \mathbf{u}^n\|_{L^2(\Omega)}^2 + \frac{2\delta t}{\mathfrak{R}e}\|\nabla\widetilde{\mathbf{u}}^{n+1}\|_{L^2(\Omega)}^2 \\ = -2\delta t\langle\nabla p^n, \widetilde{\mathbf{u}}^{n+1}\rangle - \frac{2\delta t\,\mathfrak{B}i}{\mathfrak{R}e}\langle\boldsymbol{\sigma}^{n+1}, \mathrm{D}\widetilde{\mathbf{u}}^{n+1}\rangle.\end{aligned} \tag{17}$$

The goal is to control the terms in the right-hand side (RHS) of the equality (17).

- *step 1 – control of* $\langle\boldsymbol{\sigma}^{n+1}, \mathrm{D}\widetilde{\mathbf{u}}^{n+1}\rangle$

Since $\mathbb{P}$ is a projection operator, the stress tensor $\boldsymbol{\sigma}^{n+1}$ given by the second equation of the system (9) satisfies:

$$\begin{aligned}|\boldsymbol{\sigma}^{n+1}|^2 &\leq |\boldsymbol{\sigma}^{n+1} + r\,\mathrm{D}\widetilde{\mathbf{u}}^{n+1} + \theta(\boldsymbol{\sigma}^n - \boldsymbol{\sigma}^{n+1})|^2 \\ &\leq |\boldsymbol{\sigma}^{n+1}|^2 + r^2|\mathrm{D}\widetilde{\mathbf{u}}^{n+1}|^2 + \theta^2|\boldsymbol{\sigma}^n - \boldsymbol{\sigma}^{n+1}|^2 + 2r\boldsymbol{\sigma}^{n+1} : \mathrm{D}\widetilde{\mathbf{u}}^{n+1} \\ &\quad + 2r\theta\mathrm{D}\widetilde{\mathbf{u}}^{n+1} : (\boldsymbol{\sigma}^n - \boldsymbol{\sigma}^{n+1}) + 2\theta\boldsymbol{\sigma}^{n+1} : (\boldsymbol{\sigma}^n - \boldsymbol{\sigma}^{n+1}).\end{aligned} \tag{18}$$

By invoking the Young inequality $2ab \leq a^2 + b^2$, we have

$$2r\theta\mathrm{D}\widetilde{\mathbf{u}}^{n+1} : (\boldsymbol{\sigma}^n - \boldsymbol{\sigma}^{n+1}) \leq r^2|\mathrm{D}\widetilde{\mathbf{u}}^{n+1}|^2 + \theta^2|\boldsymbol{\sigma}^n - \boldsymbol{\sigma}^{n+1}|^2,$$

and recalling the relation (16), we obtain

$$2\theta\boldsymbol{\sigma}^{n+1} : (\boldsymbol{\sigma}^n - \boldsymbol{\sigma}^{n+1}) = \theta|\boldsymbol{\sigma}^n|^2 - \theta|\boldsymbol{\sigma}^{n+1}|^2 - \theta|\boldsymbol{\sigma}^n - \boldsymbol{\sigma}^{n+1}|^2,$$

so that the inequality (18) rewrites

$$\begin{aligned}&\theta|\boldsymbol{\sigma}^{n+1}|^2 + (1-2\theta)\theta|\boldsymbol{\sigma}^{n+1} - \boldsymbol{\sigma}^n|^2 \\ &\qquad \leq 2r^2|\mathrm{D}\widetilde{\mathbf{u}}^{n+1}|^2 + 2r\boldsymbol{\sigma}^{n+1} : \mathrm{D}\widetilde{\mathbf{u}}^{n+1} + \theta|\boldsymbol{\sigma}^n|^2.\end{aligned} \tag{19}$$

After performing an integration with respect to the space variable, we obtain

$$\begin{aligned}&\theta\|\boldsymbol{\sigma}^{n+1}\|^2_{L^2(\Omega)} + (1-2\theta)\,\theta\|\boldsymbol{\sigma}^{n+1} - \boldsymbol{\sigma}^n\|^2_{L^2(\Omega)} \\ &\quad \leq 2\,r^2\|\nabla\widetilde{\mathbf{u}}^{n+1}\|^2_{L^2(\Omega)} + 2r\langle\boldsymbol{\sigma}^{n+1}, \mathrm{D}\widetilde{\mathbf{u}}^{n+1}\rangle + \theta\|\boldsymbol{\sigma}^n\|^2_{L^2(\Omega)}.\end{aligned} \tag{20}$$

- *step 2 – control of* $\langle\nabla p^n, \widetilde{\mathbf{u}}^{n+1}\rangle$

In order to estimate the pressure contribution in the RHS of (17), we proceed as follows. We take the inner product in $L^2(\Omega)^d$ of the first equation of (10) with the vector field $\frac{2(\alpha-1)\delta t}{\alpha}\mathbf{u}^{n+1}$ (which is divergence free) and use the identity (16) to derive

$$\frac{\alpha-1}{\alpha}\big(\|\mathbf{u}^{n+1}\|^2_{L^2(\Omega)} - \|\widetilde{\mathbf{u}}^{n+1}\|^2_{L^2(\Omega)} + \|\mathbf{u}^{n+1} - \widetilde{\mathbf{u}}^{n+1}\|^2_{L^2(\Omega)}\big) = 0. \tag{21}$$

We next take the inner product in $L^2(\Omega)^d$ of the same equation with the vector field $\frac{\delta t}{\alpha}(\mathbf{u}^{n+1} + \widetilde{\mathbf{u}}^{n+1})$:

$$\frac{1}{\alpha}\big(\|\mathbf{u}^{n+1}\|^2_{L^2(\Omega)} - \|\widetilde{\mathbf{u}}^{n+1}\|^2_{L^2(\Omega)}\big) + \delta t\langle\nabla(p^{n+1} - p^n), \widetilde{\mathbf{u}}^{n+1}\rangle = 0. \tag{22}$$

Finally, we take the inner product in $L^2(\Omega)^d$ of the first equation of (10), with $\delta t^2\nabla(p^{n+1} + p^n)$:

$$\alpha\,\delta t^2\big(\|\nabla p^{n+1}\|^2_{L^2(\Omega)} - \|\nabla p^n\|^2_{L^2(\Omega)}\big) - \delta t\langle\nabla(p^{n+1} + p^n), \widetilde{\mathbf{u}}^{n+1}\rangle = 0. \tag{23}$$

Adding (21), (22) and (23), we obtain:

$$\begin{aligned}\|\mathbf{u}^{n+1}\|^2_{L^2(\Omega)} + \frac{\alpha-1}{\alpha}\|\mathbf{u}^{n+1} - \widetilde{\mathbf{u}}^{n+1}\|^2_{L^2(\Omega)} + \alpha\,\delta t^2\|\nabla p^{n+1}\|^2_{L^2(\Omega)} \\ = 2\delta t\langle\nabla p^n, \widetilde{\mathbf{u}}^{n+1}\rangle + \|\widetilde{\mathbf{u}}^{n+1}\|^2_{L^2(\Omega)} + \alpha\,\delta t^2\|\nabla p^n\|^2_{L^2(\Omega)}.\end{aligned} \tag{24}$$

- *step 3 – final estimate and conclusion of the proof*

Combining the three results (17) + $\frac{\delta t\,\mathfrak{B}i}{r\,\mathfrak{R}e}$(20) + (24), we obtain

$$
\begin{aligned}
&\|\mathbf{u}^{n+1}\|^2_{L^2(\Omega)} + \frac{\delta t\,\theta\,\mathfrak{B}i}{r\,\mathfrak{R}e}\|\boldsymbol{\sigma}^{n+1}\|^2_{L^2(\Omega)} + \alpha\,\delta t^2\|\nabla p^{n+1}\|^2_{L^2(\Omega)} \\
&\quad + \frac{2\delta t}{\mathfrak{R}e}\big(1 - r\,\mathfrak{B}i\big)\|\nabla\widetilde{\mathbf{u}}^{n+1}\|^2_{L^2(\Omega)} \\
&\quad + \|\widetilde{\mathbf{u}}^{n+1} - \mathbf{u}^n\|^2_{L^2(\Omega)} + \frac{\alpha-1}{\alpha}\|\mathbf{u}^{n+1} - \widetilde{\mathbf{u}}^{n+1}\|^2_{L^2(\Omega)} \\
&\quad + \frac{\delta t(1-2\theta)\,\theta\,\mathfrak{B}i}{r\,\mathfrak{R}e}\|\boldsymbol{\sigma}^{n+1} - \boldsymbol{\sigma}^n\|^2_{L^2(\Omega)} \\
&\qquad\qquad \leq \|\mathbf{u}^n\|^2_{L^2(\Omega)} + \frac{\delta t\,\theta\,\mathfrak{B}i}{r\,\mathfrak{R}e}\|\boldsymbol{\sigma}^n\|^2_{L^2(\Omega)} + \alpha\,\delta t^2\|\nabla p^n\|^2_{L^2(\Omega)}.
\end{aligned}
\tag{25}
$$

If we denote by $y_n = \|\mathbf{u}^n\|^2_{L^2(\Omega)} + \frac{\delta t\,\theta\,\mathfrak{B}i}{r\,\mathfrak{R}e}\|\boldsymbol{\sigma}^n\|^2_{L^2(\Omega)} + \alpha\,\delta t^2\|\nabla p^n\|^2_{L^2(\Omega)}$ then the previous estimate indicates in particular that $y_{n+1} \leq y_n$ as soon as the following conditions

$$
\alpha \geq 1, \qquad 1 - r\,\mathfrak{B}i \geq 0 \quad \text{and} \quad 1 - 2\theta \geq 0
$$

hold. The sequence $(y_n)_n$ is then bounded, which implies a bound on the sequences $(\mathbf{u}^n)_n$, $(p^n)_n$ and $(\boldsymbol{\sigma}^n)_n$. Recalling (25), a bound follows on $(\widetilde{\mathbf{u}}^{n+1} - \mathbf{u}^n)_n$. As a consequence, with the help of (22), the sequence $(\widetilde{\mathbf{u}}^n)_n$ is also bounded. This completes the proof of Theorem 2 □

3.6. **Convergence results with respect to n.**

Theorem 3 (Velocity convergence)**.** *We assume that*

$$
\alpha \geq 1, \quad 3r\,\mathfrak{B}i \leq 1, \quad \theta \leq 1/3 \quad \textit{and} \quad \delta t \leq 1/2.
$$

If there exists a regular solution $(\mathbf{u}, p, \boldsymbol{\sigma})$ of (8) then the sequence $(\mathbf{u}^n)_n$ issued from the system (9)–(10) converges to $\mathbf{u}$ as n tends to $+\infty$. More precisely, there exists a constant C depending on $\mathfrak{R}e$, $\mathfrak{B}i$, r, α and T (but neither on θ nor on δt), such that for all $0 \leq n \leq N$, we have

$$
\|\mathbf{u}(t_n) - \mathbf{u}^n\|^2_{L^2(\Omega)} + \delta t\sum_{k=0}^{n}\|\mathbf{u}(t_k) - \mathbf{u}^k\|^2_{H^1(\Omega)} \leq C\,(\theta\,\delta t + \delta t^2).
$$

Remark 3.

(1) *We say that a solution $(\mathbf{u}, p, \boldsymbol{\sigma})$ of (8) is regular if we have*

$$
\begin{aligned}
&\partial_t^2\mathbf{u} \in L^2(0,T;H^{-1}(\Omega)^d), \\
&\partial_t\nabla p \in L^2(0,T;L^2(\Omega)^d), \\
&\partial_t\boldsymbol{\sigma} \in L^2(0,T;L^2(\Omega)^{d\times d}).
\end{aligned}
$$

The above assumptions for velocity and pressure are classicaly made when conducting the error analysis of the projection schemes applied to the temporal discretization of the Navier-Stokes equations (see for istance [23, 24]*).*

(2) *The error estimate derived in Theorem 3 possesses two contributions. The first one, bounded by $\theta\,\delta t$, corresponds to the error due to the "approximation" of the Bingham projection, while the second one, of the order of δt^2, is the usual error estimate obtained when time projection scheme are aplpied to the Navier-Stokes equations (see* [23, 24]*).*

(3) *The hypotheses $r\,\mathfrak{B}i \leq 1$ and $\theta \leq 1/3$ are not optimal. We will see during the sketch of the proof that these constraints on the parameters are due to use of the Young inequality $2ab \leq a^2 + b^2$. This can be improved if finer estimates are used, namely $2ab \leq \varepsilon\, a^2 + b^2/\varepsilon$ for any $\varepsilon > 0$. Nevertheless, the price to pay will be a larger numerical value of the constant C.*

Proof. Let $(\mathbf{u}, p, \boldsymbol{\sigma})$ be a regular solution of system (8) and let $(\mathbf{u}^n, \widetilde{\mathbf{u}}^n, p^n, \boldsymbol{\sigma}^n)_n$ be the solution of the discrete system (9)–(10). We introduce the following quantities

$$\begin{aligned} \mathbf{e}^n &= \mathbf{u}(t_n) - \mathbf{u}^n, \qquad & \widetilde{\mathbf{e}}^n &= \mathbf{u}(t_n) - \widetilde{\mathbf{u}}^n, \\ q^n &= p(t_n) - p^n, \qquad & \mathbf{s}^n &= \boldsymbol{\sigma}(t_n) - \boldsymbol{\sigma}^n. \end{aligned}$$

Subtracting the system (9)–(10) from the system (8) taken at time t_{n+1} leads to

$$\left\{ \begin{array}{l} \dfrac{\widetilde{\mathbf{e}}^{n+1} - \mathbf{e}^n}{\delta t} + \nabla(p(t_{n+1}) - p^n) - \dfrac{1}{\mathfrak{R}e}\Delta\widetilde{\mathbf{e}}^{n+1} = \dfrac{\mathfrak{B}i}{\mathfrak{R}e}\,\mathrm{div}\,\mathbf{s}^{n+1} + \mathrm{R}^n, \\ \dfrac{\mathbf{e}^{n+1} - \widetilde{\mathbf{e}}^{n+1}}{\delta t} - \alpha\nabla(p^{n+1} - p^n) = 0, \\ \mathrm{div}\,\mathbf{e}^{n+1} = 0, \\ \mathbf{s}^{n+1} = \mathbb{P}(\boldsymbol{\sigma}(t_{n+1}) + r\,\mathrm{D}\mathbf{u}(t_{n+1})) \\ \qquad\quad - \mathbb{P}(\boldsymbol{\sigma}^{n+1} + r\,\mathrm{D}\widetilde{\mathbf{u}}^{n+1} + \theta(\mathbf{s}^{n+1} - \mathbf{s}^n) - \theta\,\Sigma^n), \\ \widetilde{\mathbf{e}}^{n+1}\Big|_{\partial\Omega} = \mathbf{0}, \qquad \mathbf{e}^{n+1}\cdot\mathbf{n}\Big|_{\partial\Omega} = 0, \end{array} \right. \tag{26}$$

where the trunctation error terms R^n and Σ^n are given by:

$$\begin{aligned} \mathrm{R}^n &= \frac{\mathbf{u}(t_{n+1}) - \mathbf{u}(t_n)}{\delta t} - \partial_t\mathbf{u}(t_{n+1}) = \frac{1}{\delta t}\int_{t_n}^{t_{n+1}} (t_n - t)\partial_t^2\mathbf{u}(t)\,\mathrm{d}t, \\ \Sigma^n &= \sigma(t_{n+1}) - \sigma(t_n) = \int_{t_n}^{t_{n+1}} \partial_t\sigma(t)\,\mathrm{d}t. \end{aligned} \tag{27}$$

Taking the inner product in $L^2(\Omega)^d$ between the first equation of (26) and $2\delta t\,\widetilde{\mathbf{e}}^{n+1}$ and recalling (16) leads to

$$\begin{aligned} &\|\widetilde{\mathbf{e}}^{n+1}\|^2_{L^2(\Omega)} - \|\mathbf{e}^n\|^2_{L^2(\Omega)} + \|\widetilde{\mathbf{e}}^{n+1} - \mathbf{e}^n\|^2_{L^2(\Omega)} + \frac{2\delta t}{\mathfrak{R}e}\|\nabla\widetilde{\mathbf{e}}^{n+1}\|^2_{L^2(\Omega)} \\ &\qquad + 2\delta t\langle\nabla(p(t_{n+1}) - p^n), \widetilde{\mathbf{e}}^{n+1}\rangle = -\frac{2\delta t\,\mathfrak{B}i}{\mathfrak{R}e}\langle\mathbf{s}^{n+1}, \mathrm{D}\widetilde{\mathbf{e}}^{n+1}\rangle + 2\delta t\langle\mathrm{R}^n, \widetilde{\mathbf{e}}^{n+1}\rangle. \end{aligned} \tag{28}$$

We now take the inner product in $L^2(\Omega)^d$ of the second equation of (26) with $\frac{2(\alpha-1)\delta t}{\alpha}\mathbf{e}^{n+1}$, and with $\frac{\delta t}{\alpha}(\mathbf{e}^{n+1} + \widetilde{\mathbf{e}}^{n+1})$. We add the resulting relations and deduce

$$\|\mathbf{e}^{n+1}\|^2_{L^2(\Omega)} - \|\widetilde{\mathbf{e}}^{n+1}\|^2_{L^2(\Omega)} + \frac{\alpha - 1}{\alpha}\|\mathbf{e}^{n+1} - \widetilde{\mathbf{e}}^{n+1}\|^2_{L^2(\Omega)} - \delta t\langle\nabla(p^{n+1} - p^n), \widetilde{\mathbf{e}}^{n+1}\rangle = 0 \tag{29}$$

Adding equations (28) and (29), we arrive at

$$\begin{aligned}\|\mathbf{e}^{n+1}\|^2_{L^2(\Omega)} - \|\mathbf{e}^{n}\|^2_{L^2(\Omega)} + \|\widetilde{\mathbf{e}}^{n+1} - \mathbf{e}^{n}\|^2_{L^2(\Omega)} + \frac{\alpha-1}{\alpha}\|\mathbf{e}^{n+1} - \widetilde{\mathbf{e}}^{n+1}\|^2_{L^2(\Omega)} \\ + \frac{2\delta t}{\mathfrak{Re}}\|\nabla\widetilde{\mathbf{e}}^{n+1}\|^2_{L^2(\Omega)} + \delta t\langle\nabla\big(2p(t_{n+1}) - (p^{n+1}+p^n)\big), \widetilde{\mathbf{e}}^{n+1}\rangle \\ = -\frac{2\delta t\,\mathfrak{B}i}{\mathfrak{Re}}\langle\mathbf{s}^{n+1}, \mathrm{D}\widetilde{\mathbf{e}}^{n+1}\rangle + 2\delta t\langle \mathrm{R}^n, \widetilde{\mathbf{e}}^{n+1}\rangle.\end{aligned} \tag{30}$$

By introducing

$$\mathrm{Q}^n = p(t_{n+1}) - p(t_n), \tag{31}$$

we have

$$\begin{aligned}p^{n+1} - p^n &= Q^n - (q^{n+1} - q^n), \\ 2p(t_{n+1}) - (p^{n+1}+p^n) &= Q^n + (q^{n+1} + q^n).\end{aligned}$$

Taking the inner product of the second equation of (26) with $\delta t^2\nabla\big(2p(t_{n+1}) - (p^{n+1} - p^n)\big)$ and using the above relations, we derive

$$\begin{aligned}\delta t\langle\nabla\big(2p(t_{n+1}) - (p^{n+1}+p^n)\big), \widetilde{\mathbf{e}}^{n+1}\rangle = \alpha\,\delta t^2\left(\|\nabla q^{n+1}\|^2_{L^2(\Omega)} - \|\nabla q^n\|^2_{L^2(\Omega)}\right) \\ - \alpha\,\delta t^2\|\nabla\mathrm{Q}^n\|^2_{L^2(\Omega)} - 2\,\alpha\,\delta t^2\langle\nabla\mathrm{Q}^n, \nabla q^n\rangle.\end{aligned}$$

Now, by reporting this equality in (30), we obtain

$$\begin{aligned}\|\mathbf{e}^{n+1}\|^2_{L^2(\Omega)} - \|\mathbf{e}^{n}\|^2_{L^2(\Omega)} + \|\widetilde{\mathbf{e}}^{n+1} - \mathbf{e}^{n}\|^2_{L^2(\Omega)} + \frac{\alpha-1}{\alpha}\|\mathbf{e}^{n+1} - \widetilde{\mathbf{e}}^{n+1}\|^2_{L^2(\Omega)} \\ + \frac{2\delta t}{\mathfrak{Re}}\|\nabla\widetilde{\mathbf{e}}^{n+1}\|^2_{L^2(\Omega)} + \alpha\,\delta t^2\left(\|\nabla q^{n+1}\|^2_{L^2(\Omega)} - \|\nabla q^n\|^2_{L^2(\Omega)}\right) \\ = -\frac{2\delta t\,\mathfrak{B}i}{\mathfrak{Re}}\langle\mathbf{s}^{n+1}, \mathrm{D}\widetilde{\mathbf{e}}^{n+1}\rangle + 2\delta t\langle\mathrm{R}^n, \widetilde{\mathbf{e}}^{n+1}\rangle + \alpha\,\delta t^2\|\nabla\mathrm{Q}^n\|^2_{L^2(\Omega)} + 2\alpha\,\delta t^2\langle\nabla\mathrm{Q}^n, \nabla q^n\rangle.\end{aligned} \tag{32}$$

• *step 1 – control of* $\langle\mathbf{s}^{n+1}, \mathrm{D}\widetilde{\mathbf{e}}^{n+1}\rangle$

The term $\langle\mathbf{s}^{n+1}, \mathrm{D}\widetilde{\mathbf{e}}^{n+1}\rangle$ in the RHS of (32) is due to the plastic stess tensor and is a new contribution compared to the classical estimates for the projection scheme for the Stokes equations. This term is bounded as it follows. Since $\mathbb{P}$ is a projection, we have

$$|\mathbf{s}^{n+1}| \le |\mathbf{s}^{n+1} + r\,\mathrm{D}\widetilde{\mathbf{e}}^{n+1} + \theta(\mathbf{s}^n - \mathbf{s}^{n+1}) + \theta\,\Sigma^n|.$$

by taking the square of this inequality and by expanding the resulting right-hand side, we deduce

$$\begin{aligned}|\mathbf{s}^{n+1}|^2 \le |\mathbf{s}^{n+1}|^2 + r^2|\mathrm{D}\widetilde{\mathbf{e}}^{n+1}|^2 \\ + \theta^2|\mathbf{s}^n - \mathbf{s}^{n+1}|^2 + \theta^2|\Sigma^n|^2 \\ + \underbrace{2r\,\mathbf{s}^{n+1} : \mathrm{D}\widetilde{\mathbf{e}}^{n+1}}_{=a_1} + \underbrace{2\theta\,\mathbf{s}^{n+1} : (\mathbf{s}^n - \mathbf{s}^{n+1})}_{=a_2} \\ + \underbrace{2\theta\,\mathbf{s}^{n+1} : \Sigma^n}_{=a_3} + \underbrace{2r\theta\,\mathrm{D}\widetilde{\mathbf{e}}^{n+1} : (\mathbf{s}^n - \mathbf{s}^{n+1})}_{=a_4} \\ + \underbrace{2r\theta\,\mathrm{D}\widetilde{\mathbf{e}}^{n+1} : \Sigma^n}_{=a_5} + \underbrace{2\theta^2\,(\mathbf{s}^n - \mathbf{s}^{n+1}) : \Sigma^n}_{=a_6}.\end{aligned} \tag{33}$$

Note that the integral of the term a_1 with respect to the space variable $\mathbf{x} \in \Omega$ is exactly the term we aim to control. We therefore keep it unchanged. Using the identity (16), we rewrite the term a_2 as

$$a_2 = -\theta|\mathbf{s}^{n+1}|^2 + \theta|\mathbf{s}^n|^2 - \theta|\mathbf{s}^{n+1} - \mathbf{s}^n|^2.$$

With the help of the Young inequality, the term a_3 is is majorized as follows

$$a_3 \leq \theta\,\delta t|\mathbf{s}^{n+1}|^2 + \frac{\theta}{\delta t}|\Sigma^n|^2.$$

By bounding similarly the other terms in the right-hand side of (33), namely a_4, a_5 and a_6, we deduce the estimate

$$\begin{aligned}\theta(1-\delta t)|\mathbf{s}^{n+1}|^2 + \theta(1-3\theta)|\mathbf{s}^{n+1} - \mathbf{s}^n|^2 \leq\ & 2r\,\mathbf{s}^{n+1} : \mathrm{D}\widetilde{\mathbf{e}}^{n+1} \\ & + \theta|\mathbf{s}^n|^2 + 3r^2|\mathrm{D}\widetilde{\mathbf{e}}^{n+1}|^2 + \theta\,(\frac{1}{\delta t} + 3\theta)|\Sigma^n|^2.\end{aligned}$$

Integrating the above inequality with respect to the spatial variable $\mathbf{x} \in \Omega$ leads to

$$\begin{aligned}&\theta\Big[(1-\delta t)\|\mathbf{s}^{n+1}\|^2_{L^2(\Omega)} - \|\mathbf{s}^n\|^2_{L^2(\Omega)}\Big] + \theta(1-3\theta)\|\mathbf{s}^{n+1} - \mathbf{s}^n\|^2_{L^2(\Omega)} \\ &\qquad \leq\ 2r\,\langle \mathbf{s}^{n+1}, \mathrm{D}\widetilde{\mathbf{e}}^{n+1}\rangle + 3r^2\|\mathrm{D}\widetilde{\mathbf{e}}^{n+1}\|^2_{L^2(\Omega)} + \theta\,(\frac{1}{\delta t} + 3\theta)\|\Sigma^n\|^2_{L^2(\Omega)}.\end{aligned} \tag{34}$$

• *step 2 – final estimate*

By combining the three results (32) + $\frac{\delta t\,\mathfrak{B}i}{r\,\mathfrak{R}e}$(34) and recalling that $\|D\widetilde{\mathbf{e}}^{n+1}\|_{L^2(\Omega)} \leq \|\nabla\widetilde{\mathbf{e}}^{n+1}\|_{L^2(\Omega)}$, we obtain

$$\begin{aligned}&\|\mathbf{e}^{n+1}\|^2_{L^2(\Omega)} - \|\mathbf{e}^n\|^2_{L^2(\Omega)} + \frac{\alpha-1}{\alpha}\|\mathbf{e}^{n+1} - \widetilde{\mathbf{e}}^{n+1}\|^2_{L^2(\Omega)} \\ &\quad + \|\widetilde{\mathbf{e}}^{n+1} - \mathbf{e}^n\|^2_{L^2(\Omega)} + \frac{\delta t}{\mathfrak{R}e}(2 - 3r\,\mathfrak{B}i)\|\nabla\widetilde{\mathbf{e}}^{n+1}\|^2_{L^2(\Omega)} \\ &\quad + \frac{\theta\,\delta t\,\mathfrak{B}i}{r\,\mathfrak{R}e}\Big[(1-\delta t)\|\mathbf{s}^{n+1}\|^2_{L^2(\Omega)} - \|\mathbf{s}^n\|^2_{L^2(\Omega)}\Big] \\ &\quad + \frac{\theta(1-3\theta)\,\delta t\,\mathfrak{B}i}{r\,\mathfrak{R}e}\|\mathbf{s}^{n+1} - \mathbf{s}^n\|^2_{L^2(\Omega)} \\ &\quad + \alpha\,\delta t^2\Big[\|\nabla q^{n+1}\|^2_{L^2(\Omega)} - \|\nabla q^n\|^2_{L^2(\Omega)}\Big] \\ &\qquad \leq \underbrace{2\delta t\langle \mathrm{R}^n, \widetilde{\mathbf{e}}^{n+1}\rangle}_{b_1} + \theta\,(1+3\theta\,\delta t)\,\frac{\mathfrak{B}i}{r\,\mathfrak{R}e}\|\Sigma^n\|^2_{L^2(\Omega)} \\ &\qquad\quad + \alpha\,\delta t^2\|\nabla \mathrm{Q}^n\|^2_{L^2(\Omega)} + \underbrace{2\alpha\,\delta t^2\langle \nabla \mathrm{Q}^n, \nabla q^n)\rangle}_{b_2}.\end{aligned} \tag{35}$$

The term b_1 is treated by invoking the duality between H^{-1} and H^1_0, and the Young inequality, so that

$$\begin{aligned}b_1 &\leq 2\delta t\|\mathrm{R}^n\|_{H^{-1}(\Omega)}\|\widetilde{\mathbf{e}}^{n+1}\|_{H^1_0(\Omega)} \\ &\leq \frac{\delta t}{\mathfrak{R}e}\|\nabla\widetilde{\mathbf{e}}^{n+1}\|^2_{L^2(\Omega)} + \delta t\,\mathfrak{R}e\,\|\mathrm{R}^n\|^2_{H^{-1}(\Omega)}.\end{aligned}$$

The term b_2 is majorized using the Young inequality as follows

$$\begin{aligned}b_2 &\leq 2\,\alpha\,\delta t^2\,\|\nabla \mathrm{Q}^n\|_{L^2(\Omega)}\|\nabla q^n\|_{L^2(\Omega)} \\ &\leq \alpha\,\delta t\|\nabla \mathrm{Q}^n\|^2_{L^2(\Omega)} + \alpha\,\delta t^3\|\nabla q^n\|^2_{L^2(\Omega)}\end{aligned}$$

Reporting these bounds on b_1 and b_2 in (35), we obtain

$$
\begin{aligned}
&\|\mathbf{e}^{n+1}\|^2_{L^2(\Omega)} - \|\mathbf{e}^{n}\|^2_{L^2(\Omega)} + \frac{\alpha-1}{\alpha}\|\mathbf{e}^{n+1} - \widetilde{\mathbf{e}}^{n+1}\|^2_{L^2(\Omega)} \\
&\quad + \|\widetilde{\mathbf{e}}^{n+1} - \mathbf{e}^{n}\|^2_{L^2(\Omega)} + \frac{\delta t}{\mathfrak{Re}}(1 - 3r\,\mathfrak{Bi})\|\nabla\widetilde{\mathbf{e}}^{n+1}\|^2_{L^2(\Omega)} \\
&\quad + \frac{\theta\,\delta t\,\mathfrak{Bi}}{r\,\mathfrak{Re}}\Big[(1-\delta t)\|\mathbf{s}^{n+1}\|^2_{L^2(\Omega)} - \|\mathbf{s}^{n}\|^2_{L^2(\Omega)}\Big] \\
&\quad + \frac{\theta(1-3\theta)\,\delta t\,\mathfrak{Bi}}{r\,\mathfrak{Re}}\|\mathbf{s}^{n+1} - \mathbf{s}^{n}\|^2_{L^2(\Omega)} \\
&\quad + \alpha\,\delta t^2\Big[\|\nabla q^{n+1}\|^2_{L^2(\Omega)} - \|\nabla q^{n}\|^2_{L^2(\Omega)}\Big] \\
&\qquad\qquad \leq \delta t\,\mathfrak{Re}\,\|\mathrm{R}^n\|^2_{H^{-1}(\Omega)} + \theta\,(1+3\theta\,\delta t)\,\frac{\mathfrak{Bi}}{r\,\mathfrak{Re}}\|\Sigma^n\|^2_{L^2(\Omega)} \\
&\qquad\qquad + \alpha\,\delta t\,(1+\delta t)\,\|\nabla\mathrm{Q}^n\|^2_{L^2(\Omega)} + \alpha\,\delta t^3\|\nabla\mathrm{q}^n\|^2_{L^2(\Omega)}.
\end{aligned}
\tag{36}
$$

• *step 3 – The Gronwall lemma*
If the following conditions

$$
\alpha \geq 1, \qquad 3r\,\mathfrak{Bi} \leq 1, \qquad \theta \leq 1/3,
$$

hold, we deduce from the above inequality

$$
y_{n+1} + z_{n+1} \leq \frac{(1+\delta t)}{(1-\delta t)}\,y_n + \varepsilon_n,
\tag{37}
$$

where

$$
\begin{aligned}
y_n &= (1-\delta t)\left(\|\mathbf{e}^n\|^2_{L^2(\Omega)} + \frac{\mathfrak{Bi}}{r\,\mathfrak{Re}}\,\theta\,\delta t\,\|\mathbf{s}^n\|^2_{L^2(\Omega)} + \alpha\delta t^2\,\|\nabla q^n\|^2_{L^2(\Omega)}\right) \\
z_n &= \frac{(1-3r\mathfrak{Bi})}{\mathfrak{Re}}\,\delta t\,\|\nabla\widetilde{\mathbf{e}}^{n+1}\|^2_{L^2(\Omega)}
\end{aligned}
$$

and

$$
\varepsilon_n = \delta t\mathfrak{Re}\,\|\mathrm{R}^n\|^2_{H^{-1}(\Omega)} + \theta(1+3\theta\,\delta t)\,\frac{\mathfrak{Bi}}{r\,\mathfrak{Re}}\,\|\Sigma^n\|^2_{L^2(\Omega)} + \alpha\,\delta t\,(1+\delta t)\,\|\nabla\mathrm{Q}^n\|^2_{L^2(\Omega)}.
$$

By applying the discrete Gronwall lemma to (37), we derive, for any $1 \leq m \leq N$,

$$
y_m + \sum_{j=1}^{m} z_j \leq \left(\frac{1+\delta t}{1-\delta t}\right)^m \left(y_0 + \sum_{n=0}^{m-1}\varepsilon_n\right).
$$

Noting that, for $\delta t \leq \frac{1}{2}$, we have $\frac{1+\delta t}{1-\delta t} \leq (1+\delta t)^3 \leq \exp(3\delta t)$, then for all $1 \leq m \leq N$, the following inequality holds

$$
y_m + \sum_{n=1}^{m} z_n \leq e^{3T}\left(y_0 + \sum_{n=0}^{m-1}\varepsilon_n\right).
\tag{38}
$$

Recalling that, by definition, $\mathbf{e}^0 = 0$ the proof of the theorem relies on deriving a proper bound for the term $\sum_{j=0}^{n-1}\varepsilon_j$ in the above inequality.

• *step 4 – control of the error* ε_n

We now derive estimates of the term ε_n with respect to the parameters θ and δt. From the definition of Σ^n (in (27)), we have

$$\|\Sigma^n\|^2_{L^2(\Omega)} = \Big\| \int_{t_n}^{t_{n+1}} \partial_t \sigma(t)\,\mathrm{d}t \Big\|^2_{L^2(\Omega)} \leq \delta t \int_{t_n}^{t_{n+1}} \|\partial_t \sigma(t)\|^2_{L^2(\Omega)}\,\mathrm{d}t,$$

similarly for Q^n (in (31)), we obtain

$$\|\nabla \mathrm{Q}^n\|^2_{L^2(\Omega)} \leq \delta t \int_{t_n}^{t_{n+1}} \|\partial_t \nabla p\|^2_{L^2(\Omega)}\,\mathrm{d}t,$$

and finally for R^n (in (27)),, we have

$$\begin{aligned}
\|\mathrm{R}^n\|^2_{H^{-1}(\Omega)} &= \frac{1}{\delta t^2}\Big\| \int_{t_n}^{t_{n+1}} (t_n - t)\partial_t^2 \mathbf{u}(t)\,\mathrm{d}t \Big\|^2_{H^{-1}(\Omega)} \\
&\leq \frac{1}{\delta t^2}\Big(\int_{t_n}^{t_{n+1}} (t - t_n)^2\,\mathrm{d}t \Big)\Big(\int_{t_n}^{t_{n+1}} \|\partial_t^2 \mathbf{u}(t)\|^2_{H^{-1}(\Omega)}\,\mathrm{d}t \Big) \\
&\leq \frac{\delta t}{3} \int_{t_n}^{t_{n+1}} \|\partial_t^2 \mathbf{u}(t)\|^2_{H^{-1}(\Omega)}\,\mathrm{d}t.
\end{aligned}$$

Reporting these estimates in the above definition of ε_n, assuming the regularity of the solution $(\mathbf{u}, p, \sigma)$ and summing up from $n = 0$ to $m - 1$, leads to

$$\begin{aligned}
\sum_{n=0}^{m-1} \varepsilon_n \leq \delta t^2 \left(\frac{\mathfrak{Re}}{3} \|\partial_t^2 \mathbf{u}\|^2_{L^2(0,T;H^{-1}(\Omega)^d)} + \alpha\,(1 + \delta t)\|\partial_t \nabla p\|^2_{L^2(0,T;L^2(\Omega)^d)} \right) \\
+ \theta\,\delta t\,(1 + 3\theta\,\delta t)\,\frac{\mathfrak{Bi}}{r\,\mathfrak{Re}}\,\|\partial_t \sigma\|^2_{L^2(0,T;L^2(\Omega)^{d\times d})}.
\end{aligned} \tag{39}$$

• *step 6 – Conclusion of the proof*

Thanks to (39), the inequality (38) now reads, for all $1 \leq m \leq N$,

$$y_m + \sum_{n=1}^{m} z_n \leq \exp(3\mathrm{T}) \Big(c_1\,\theta\,\delta t + c_2\,\delta t^2 \Big) \tag{40}$$

with

$$\begin{cases}
c_1 = \dfrac{\mathfrak{Bi}}{r\,\mathfrak{Re}} \Big(\|\mathbf{s}^0\|^2_{L^2(\Omega)} + \dfrac{3}{2}\,\|\partial_t \sigma\|^2_{L^2(0,T;L^2(\Omega)^{d\times d})} \Big), \\
c_2 = \dfrac{\mathfrak{Re}}{3}\,\|\partial_t^2 \mathbf{u}\|^2_{L^2(0,T;H^{-1}(\Omega)^d)} + \dfrac{3\alpha}{2}\,\|\partial_t \nabla p\|^2_{L^2(0,T;L^2(\Omega)^d)} + \alpha \|\nabla q^0\|^2_{L^2(\Omega)},
\end{cases}$$

Recalling the definition of y_n and z_n, and that $1 - \delta t \geq \frac{1}{2}$, we deduce that

$$\|\mathbf{e}^n\|^2_{L^2(\Omega)} \leq 2\exp(3T) \Big(c_1\,\theta\,\delta t + c_2\,\delta t^2 \Big),$$

and

$$\delta t \sum_{j=1}^{n} \|\nabla \widetilde{\mathbf{e}}^j\|^2_{L^2(\Omega)} \leq \frac{\mathfrak{Re}}{(1 - 3r\mathfrak{Bi})} \exp(3T) \Big(c_1\,\theta\,\delta t + c_2\,\delta t^2 \Big).$$

Thanks to the inequality (see [25, Remark 1.6])

$$\|\mathbf{e}^n\|_{H^1(\Omega)} \leq C(\Omega) \|\widetilde{\mathbf{e}}^n\|_{H^1(\Omega)}$$

we conclude the proof of Theorem 3. □

3.7. **Some remarks.**

✓ *Convergence of the velocity*

Theorem 3 can be interpreted in several ways. The first one shows that, selecting θ of order δt, the discrete velocity field is a first-order approximation of the solution $\mathbf{u}$ of the Stokes-Bingham equation (8). The second one proves that, for a fixed value of the parameter θ (satisfying the assumption $\theta \leq 1/3$), the scheme converges to the solution of the Stokes-Bingham problem (8). This important property shows that our projection scheme (9)–(10)–(11) is very different than the common regularization method, studied for instance in [27], which rewrites the plastic tensor as

$$\boldsymbol{\sigma}_\varepsilon = \frac{\mathrm{D}\mathbf{u}}{\sqrt{|\mathrm{D}\mathbf{u}|^2 + \varepsilon^2}} \quad \text{instead of} \quad \boldsymbol{\sigma} = \frac{\mathrm{D}\mathbf{u}}{|\mathrm{D}\mathbf{u}|}.$$

Indeed, the error derived for the regularized problem is cumulative, that is bounded by $\delta t + \sqrt{\varepsilon}$ (see Theorem 4.7 [27]), while the error obtained in Theorem 3 is bounded by $\delta t\,(\theta + \delta t)$. The discrete velocity field solution of our projection scheme converges to the solution of the Stokes-Bingham equations wathever the value of θ is. In the following section, we will also see that the projection scheme proposed in the present article captures the flow cessation property in finite time characterizing viscoplastic Bingham flows.

✓ *Convergence of the stress tensor*

Obviously, Theorem 3 does not provide a convergence result for the stress tensor sequence. Nevertheless, the sequence $(\boldsymbol{\sigma}^n)_n$ is well defined and bounded so that we have a convergence up to a subsequence. However, we can prove the following result:
The sequence $(\boldsymbol{\sigma}^n)_n$ satisfies

$$\|\boldsymbol{\sigma}_{\delta t}(t_n) - \boldsymbol{\sigma}^n\|^2_{L^2(\Omega)} \leq C\delta t, \tag{41}$$

where $(\mathbf{u}_{\delta t}, p_{\delta t}, \boldsymbol{\sigma}_{\delta t})$ is the solution of

$$\begin{cases} \partial_t \mathbf{u}_{\delta t} + \mathbf{u}_{\delta t} \cdot \nabla \mathbf{u}_{\delta t} + \nabla p_{\delta t} - \dfrac{1}{\mathfrak{R}e} \Delta \mathbf{u}_{\delta t} = \dfrac{\mathfrak{B}i}{\mathfrak{R}e} \operatorname{div} \boldsymbol{\sigma}_{\delta t}, \\ \operatorname{div} \mathbf{u}_{\delta t} = 0, \\ \boldsymbol{\sigma}_{\delta t} = \mathbb{P}(\boldsymbol{\sigma}_{\delta t} + r\,\mathrm{D}\mathbf{u}_{\delta t} - \delta t\,\theta\,\partial_t \boldsymbol{\sigma}_{\delta t}). \end{cases} \tag{42}$$

Indeed the proof is very similar to the one of Theorem 3. The only change is in the value of the residual tensor which becomes

$$\widehat{\Sigma}^n = \boldsymbol{\sigma}(t_{n+1}) - \boldsymbol{\sigma}(t_n) - \delta t\,\partial_t \boldsymbol{\sigma}_{\delta t}(t_{n+1}) = \int_{t_n}^{t_{n+1}} (t_n - t) \partial_t^2 \boldsymbol{\sigma}_{\delta t}(t)\,\mathrm{d}t.$$

Under some regularity assumptions on $\boldsymbol{\sigma}_{\delta t}$, we deduce that

$$\begin{aligned} \sum_{n=0}^{N} \|\widehat{\Sigma}^n\|^2_{L^2(\Omega)} &= \sum_{n=0}^{N} \Big\| \int_{t_n}^{t_{n+1}} (t_n - t) \partial_t \boldsymbol{\sigma}(t)\,\mathrm{d}t \Big\|^2_{L^2(\Omega)} \\ &\leq \sum_{n=0}^{N} \Big(\int_{t_n}^{t_{n+1}} (t - t_n)\,\mathrm{d}t \Big) \Big(\int_{t_n}^{t_{n+1}} (t - t_n) \|\partial_t \boldsymbol{\sigma}(t)\|^2_{L^2(\Omega)}\,\mathrm{d}t \Big) \\ &\leq \frac{\delta t^2}{2} \int_0^T t\,\|\partial_t \boldsymbol{\sigma}(t)\|^2_{L^2(\Omega))}\,\mathrm{d}t \lesssim \delta t^2. \end{aligned}$$

In this case, the cumulative error $\sum_{n=0}^{N-1}\varepsilon_n$ satisfies

$$\sum_{n=0}^{N-1}\varepsilon_n \leq C\delta t^2,$$

where C is an appropriate constant depending on the datas and on the solution $(\mathbf{u},p)$ of the Stokes-Bingham problem. This result implies the result (41).
Note also that with this error estimate on the stress tensor, we may expect to obtain an estimate of convergence on the pressure like (see theorem 2 on page 72 in [23] and [24] for the proof):

$$\delta t\sum_{k=0}^{n}\|p_{\delta t}(t_n)-p^n\|^2_{L^2(\Omega)} \leq C\,\delta t^2. \tag{43}$$

4. Numerical results on a more complex scheme

In this section we present numerical simulations of solutions of the following equations modelling the motion of an incompressible Bingham viscoplastic medium:

$$\begin{cases} \partial_t\mathbf{u}-\dfrac{1}{\mathfrak{Re}}\Delta\mathbf{u}+\operatorname{div}(\mathbf{u}\otimes\mathbf{u})+\nabla p=\dfrac{\mathfrak{Bi}}{\mathfrak{Re}}\operatorname{div}\boldsymbol{\sigma},\\ \operatorname{div}\mathbf{u}=0,\\ \boldsymbol{\sigma}=\mathbb{P}(\boldsymbol{\sigma}+r\,\mathrm{D}\mathbf{u}),\\ \mathbf{u}|_{\partial\Omega}=\mathbf{u}_b, \end{cases} \tag{44}$$

where $\mathbf{u}_b$ is prescribed and defined on the domain boundary $\partial\Omega$. We denote by (u,v) the components of the velocity field $\mathbf{u}$. Note that the conservative form of the nonlinearity is used. We also introduce $\mathbf{e}_1=(1,0)$ and $\mathbf{e}_2=(0,1)$.

4.1. Description of the time and space discretization.

Temporal discretization. Instead of the first-order time scheme (9)–(10) studied in the previous section, we have implemented a second-order projection method based on the combination of the BDF2 (second-order Backward Differentiation Formulae) and the AB2 (Adams–Bashforth) schemes (see [12] for instance). For $n\geq 0$, assuming that $\mathbf{u}^n$, $\boldsymbol{\sigma}^n$ and p^n are known, the computation of $(\mathbf{u}^{n+1},\boldsymbol{\sigma}^{n+1},p^{n+1})$ consists in:

✓ Computing $\boldsymbol{\sigma}^{n+1}$ and a velocity predictor $\widetilde{\mathbf{u}}^{n+1}$ by solving:

$$\begin{cases} \dfrac{3\widetilde{\mathbf{u}}^{n+1}-4\mathbf{u}^n+\mathbf{u}^{n-1}}{2\delta t}-\dfrac{1}{\mathfrak{Re}}\Delta\widetilde{\mathbf{u}}^{n+1}-\dfrac{\mathfrak{Bi}}{\mathfrak{Re}}\operatorname{div}\boldsymbol{\sigma}^{n+1}=-\nabla p^n-2\operatorname{div}(\mathbf{u}^n\otimes\mathbf{u}^n)\\ \qquad\qquad +\operatorname{div}(\mathbf{u}^{n-1}\otimes\mathbf{u}^{n-1}),\\ \widetilde{\mathbf{u}}^{n+1}\Big|_{\partial\Omega}=\mathbf{u}_b,\\ \boldsymbol{\sigma}^{n+1}=\mathbb{P}\big(\boldsymbol{\sigma}^{n+1}+r\,\mathrm{D}\widetilde{\mathbf{u}}^{n+1}+\theta(\boldsymbol{\sigma}^n-\boldsymbol{\sigma}^{n+1})\big). \end{cases} \tag{45}$$

✓ Projecting $\widetilde{\mathbf{u}}^{n+1}$ to obtain a divergence-free velocity field $\mathbf{u}^{n+1}$ and the pressure p^{n+1}:

$$\begin{cases} \dfrac{3(\mathbf{u}^{n+1}-\widetilde{\mathbf{u}}^{n+1})}{2\delta t}+\nabla(p^{n+1}-p^n)=\mathbf{0},\\ \operatorname{div}\mathbf{u}^{n+1}=0,\\ (\mathbf{u}^{n+1}-\widetilde{\mathbf{u}}^{n+1})\cdot\mathbf{n}\Big|_{\partial\Omega}=0. \end{cases} \tag{46}$$

Remark 4. *In practice,* (46) *is solved in two steps. First,* $\mathbf{u}^{n+1}$ *is eliminated from the first equation using the incompressibility constraint. This results in a system relating* p^{n+1} *to the predicted velocity field* $\widetilde{\mathbf{u}}^{n+1}$ *and to* p^n*. Once the new pressure has been computed,* $\mathbf{u}^{n+1}$ *is updated wih the help of the first equation. Note that in order to recover an almost, i.e up to the computer accuracy, solenoidal velocity field this process should be applied at the fully discrete level, meaning after the space discretization has been performed on* (46)*.*

Space discretization. The computational domain $\Omega = (0, L_x) \times (0, L_y)$ is discretized by using a cartesian uniform mesh. Let N_x and N_y be the number of mesh cells in the x and y directions, we define the grid points by

$$x_i = (i-1)\, h_x \ \text{ for } \ i = 1, \ldots, N_x + 1,$$
$$y_j = (j-1)\, h_y \ \text{ for } \ j = 1, \ldots, N_y + 1,$$

where $h_x = L_x/N_x$ and $h_y = L_y/N_y$. With the mesh points x_i and y_j, we associate the midpoints

$$x_{i+1/2} = \frac{1}{2}(x_{i+1} + x_i) \ \text{ for } \ i = 1, \ldots, N_x,$$
$$y_{j+1/2} = \frac{1}{2}(y_{j+1} + y_j) \ \text{ for } \ j = 1, \ldots, N_y.$$

Let a computational cell $K_{ij} = (x_i, x_{i+1}) \times (y_j, y_{j+1})$. As in the classical MAC scheme for the incompressible Navier-Stokes equations (see [13]) the discrete velocity unknowns u_{ij} and v_{ij} are located at the midpoint of the cell edges, that is $u_{ij} \approx u(x_i, y_{j+1/2})$ and $v_{ij} \approx v(x_{i+1/2}, y_j)$. The discrete pressure p_{ij} as well as the discrete extra-stress tensor $\boldsymbol{\sigma}_{ij}$ are placed at the center $(x_{i+1/2}, y_{j+1/2})$ of the mesh cell K_{ij}. Figure 1 summarizes this staggered arrangement of the unknowns.

The spatial discretization of (45) and (46) is achieved by integrating the equation of the horizontal (resp. vertical) velocity component over the control volume $K_{i,j+1/2} = (x_{i-1/2}, x_{i+1/2}) \times (y_j, y_{j+1})$ (resp. $K_{i+1/2,j} = (x_i, x_{i+1}) \times (y_{j-1/2}, y_{j+1/2})$). Classical cell-centered second-order finite volume schemes are applied to discretize all first and second-order partial derivatives with respect to the spatial directions.

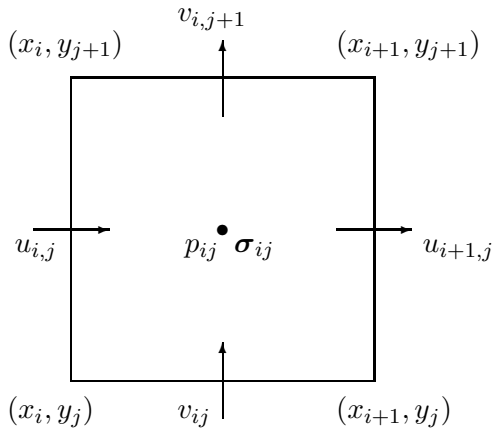

FIGURE 1. Location of the discrete unknowns in the mesh cell $K_{ij} = (x_i, x_{i+1}) \times (y_j, y_{j+1})$.

Boundary conditions. Additional mesh points are added outside of the computational domain, namely:

$$x_{1/2} \,=\, x_1 - \frac{h_x}{2}, \quad x_{N_x+3/2} \,=\, x_{N_x+1} + \frac{h_x}{2}$$

and similarly for y. *Ghost* values are associated with these extra mesh points in order to enforce the boundary conditions, for instance we introduce the additional velocity value $u_{i,0}$ and enforce a Dirichlet boundary condition by setting

$$\frac{u_{i,0} + u_{i,1}}{2} \,=\, u_b(x_i, 0).$$

A second-order approximation of the boundary condition is therefore employed. Note that Neumann boundary conditions can be handled similarly.

As the spatial discretization of the Navier-Stokes equations on a staggered grid is well known, details are ommited in the sequel. However, we provide the discrete formulae applied to the terms in (45)-(46) depending on the stress tensor $\boldsymbol{\sigma}$.

The momentum equation. For $j = 1, \ldots, N_y$ and $i = 2, \ldots, N_x$, the discrete contribution of the extra-stress tensor in the horizontal momentum equation writes

$$\begin{aligned}
\int_{K_{i,j+1/2}} \operatorname{div} \boldsymbol{\sigma} \cdot \mathbf{e}_1 \, d\mathbf{x} \,&=\, \int_{y_j}^{y_{j+1}} \big(\sigma_{11}(x_{i+1/2}, y) - \sigma_{11}(x_{i-1/2}, y)\big)\, dy \\
&\qquad + \int_{x_{i-1/2}}^{x_{i+1/2}} \big(\sigma_{12}(x, y_{j+1}) - \sigma_{12}(x, y_j)\big)\, dx, \\
&\approx\, h_y\big(\sigma_{11}(x_{i+1/2}, y_{j+1/2}) - \sigma_{11}(x_{i-1/2}, y_{j+1/2})\big) \\
&\qquad + h_x\big(\sigma_{12}(x_i, y_{j+1}) - \sigma_{12}(x_i, y_j)\big), \\
&\approx\, h_y\big(\sigma_{11}|_{i,j} - \sigma_{11}|_{i-1,j}\big) + h_x\big(\overline{\sigma_{12}}|_{i,j+1} - \overline{\sigma_{12}}|_{i,j}\big),
\end{aligned}$$

where $\overline{\sigma_{12}}|_{i,j}$ denotes a second-order approximation of σ_{12} at the mesh point (x_i, y_j) namely we use

$$\overline{\sigma_{12}}|_{i,j} \,=\, \begin{cases}
\dfrac{3}{2}\big(\sigma_{12}|_{i-1,1} + \sigma_{12}|_{i,1}\big) - \dfrac{1}{2}\big(\sigma_{12}|_{i-1,2} + \sigma_{12}|_{i,2}\big) & \text{for } \; j = 1, \\
\dfrac{1}{4}\big(\sigma_{12}|_{i-1,j-1} + \sigma_{12}|_{i-1,j} + \sigma_{12}|_{i,j} + \sigma_{12}|_{i,j-1}\big) & \text{for } \; j = 2, \ldots, N_y, \\
\dfrac{3}{2}\big(\sigma_{12}|_{i-1,N_y} + \sigma_{12}|_{i,N_y}\big) - \dfrac{1}{2}\big(\sigma_{12}|_{i,N_y-1} + \sigma_{12}|_{i-1,N_y-1}\big) & \text{for } \; j = N_y + 1.
\end{cases}$$

The Bingham-projection. As discrete velocity and extra-stress tensor are staggered, the computation of the diagonal components of the deformation tensor $\mathrm{D}\widetilde{\mathbf{u}}^{n+1}$ in (45) is straightforward : second-order centered formulae are used. The off-diagonal term, involving cross partial devivatives, requires specific formulae for mesh points in the vicinity of the domain boundary, namely for $i = 1, \ldots, N_x$, we use

$$\frac{\partial u}{\partial y}(x_{i+1/2}, y_{j+1/2}) \,\approx\, \begin{cases}
\big(3\,\overline{u}_{i+1/2,1/2} - 4\,\overline{u}_{i+1/2,0} + \overline{u}_{i+1/2,3/2}\big)/(3h_y) & \text{for } \; j = 1, \\
\big(\overline{u}_{i+1/2,j+3/2} - \overline{u}_{i+1/2,j-1/2}\big)/(2h_y) & \text{for } \; j = 2, \ldots, N_y - 1, \\
\big(-\overline{u}_{i+1/2,N_y-1/2} + 4\,\overline{u}_{i+1/2,N_y+1} - 3\,\overline{u}_{i+1/2,N_y+1/2}\big)/(3h_y) & \text{for } \; j = N_y,
\end{cases}$$

where $\overline{u}_{i+1/2,j+1/2}$ is the following second-order interpolation

$$\overline{u}_{i+1/2,j+1/2} = \frac{u_{i,j} + u_{i,j+1}}{2}$$

completed with the boundary conditions

$$\overline{u}_{i+1/2,0} = u(x_{i+1/2}, 0) \quad \text{and} \quad \overline{u}_{i+1/2,N_y+1} = u(x_{i+1/2}, L_y).$$

Similar formulae are employed to approximate $\frac{\partial v}{\partial x}(x_{i+1/2}, y_{j+1/2})$ which completes the discretization scheme for $\left(\mathrm{D}\widetilde{\mathbf{u}}^{n+1}\right)_{12}$.

This numerical scheme has been implemented in a F90/MPI code simulating Newtonian flows. The PETSc library [1, 2] is used to solve the linear systems and to manage datas on structured grids. The communications beween the MPI processes are written explicitely by using routines of the MPI library. All the numerical simulations presented in the following sections have been conducted by using from 4 up to 16 MPI processes.

4.2. **Stationary flows in the lid-driven cavity at $\mathfrak{Re} = 10^3$.** In order to validate our numerical scheme, we attempt to reproduce some of the benchmark results provided in [26] for stationary viscoplastic flows in a lid-driven cavity at Reynolds number $\mathfrak{Re} = 10^3$ and Bingham numbers in the range $\mathfrak{Bi} \in [0, 100]$. The lid-driven cavity consists in the computational domain $\Omega = (0, 1)^2$ and in the boundary conditions

$$\mathbf{u}_b = \begin{cases} (1,0) & \text{on the top boundary } y = 1, \\ (0,0) & \text{elsewhere.} \end{cases}$$

We assume that a stationary state is reached when the following criterion is satisfied

$$\frac{\|\mathbf{u}^{n+1} - \mathbf{u}^n\|_\infty}{\delta t} \leq 10^{-6},$$

where the time step is chosen so that the CFL number, namely $\delta t \|\mathbf{u}^{n+1}\|_\infty / h$, is equal to unity. In this computational set up the mesh sizes satisfy $h_x = h_y = h$. We first validate our numerical code against the results provided by Botella and Peyret in [4] for Newtonian fluid flows ($\mathfrak{Bi} = 0$). In Table 1, extrema values and locations of the horizontal (resp. vertical) velocity component along the vertical (resp. horizontal) centerline are reported for mesh resolutions from 256^2 up to 1024^2. We note a very good agreement between our values and the values listed in [4]. Moreover, by comparing the results obtained on the different meshes we find that the expected second-order accuracy is recovered. Also a perfect match of the velocity profiles drawn on Figures 2 and 3 is found with the values provided by Botella and Peyret in [4]. We now turn to the validation of our numerical method for viscoplastic fluid flows against the results obtained by Vola et al. and reported in [26]. The Bingham projection procedure depends on two parameters : r and θ. The former one is set to fulfill the necessary condition exhibited in Theorem 3, that is: $r \leq \frac{1}{3\mathfrak{Bi}}$. The time relaxation parameter θ is set equal to the time step δt. The convergence of the sequence $\left\{\boldsymbol{\sigma}^{n,k},\, k \geq 0\right\}$ in the Bingham projection procedure (11) is considered to be reached when the following criterium is satisfied:

$$|\boldsymbol{\sigma}^{n,k+1} - \boldsymbol{\sigma}^{n,k}| \leq 10^{-10}.$$

An overall good agreement is found for the values reported in Table 1: the differences between our results and the ones in [26] are smaller than the accuracy of the numerical scheme, that is $O(h^2)$, for $\mathfrak{Bi} \leq 10$. A discripency is found for the values of $\min_x v(x, y = 0.5)$ and $\max_x v(x, y =$

0.5) at the largest Bingham number $\mathfrak{B}i = 100$. The net effect of the extra yield-stress tensor is to slow down the flow motion so that we may expect that coarser mesh resolutions could be used when the Bingham number is increased. However, at the interface between the motion and rigid zones, which appear in viscoplastic medium, very large velocity gradients are encountered. In order to compute accurately these sharp gradients, the mesh resolution has to be fine enough. This is clearly observed by seeking at the values of $\min_x v(x, y = 0.5)$ and $\max_x v(x, y = 0.5)$ at $\mathfrak{B}i = 100$ for increasing mesh resolutions. We infer from these results that 512^2 grid points are necessary to compute the correct order of magnitude for these characteristic and that the observed differences with [26] are due to the use of a much finer resolution in the present numerical simulations.

Finally, on Figure 4 the streamlines and the rigid zones, that are aeras where the deformation tensor vanishes, are drawn for the different values of the Bingham number. By comparing with Figure 4 in [26]

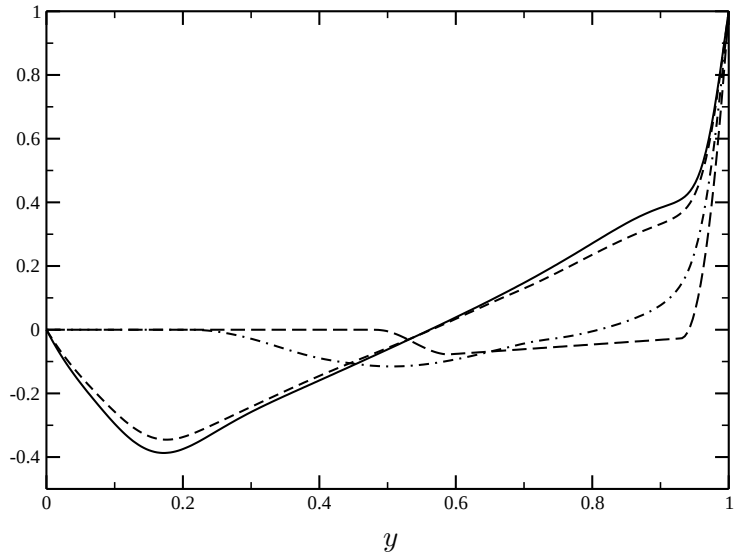

FIGURE 2. Horizontal velocity profiles along the centerline $x = 0.5$ for stationnary solutions at $\mathfrak{R}e = 10^3$ and for $\mathfrak{B}i = 0$ (——), $\mathfrak{B}i = 1$ (- - -), $\mathfrak{B}i = 10$ (·- - -) and $\mathfrak{B}i = 100$ (– – –).

4.3. **Numerical estimates of the covergence rate.** In order to estimate the convergence rate of our numerical scheme with respect to both the spatial and temporal discretizations, we have performed simulations of a viscoplastic medium flow at $\mathfrak{R}e = 10^3$ and $\mathfrak{B}i = 1$ in a regularized lid-driven cavity. The computational domain is $\Omega = (0, 1)^2$ and the top boundary condition is:

$$\mathbf{u}_b(x, 1) = \left(\left(1 - (2x - 1)^2\right)^2, 0\right).$$

Simulations on computational grids ranging from 32^2 up to 2048^2 mesh points have been done. The time integration has been conducted up to $t = 1$ with a time step being equal to the mesh size, so that the CFL number approximatively equals unity. The flow motion is far from being

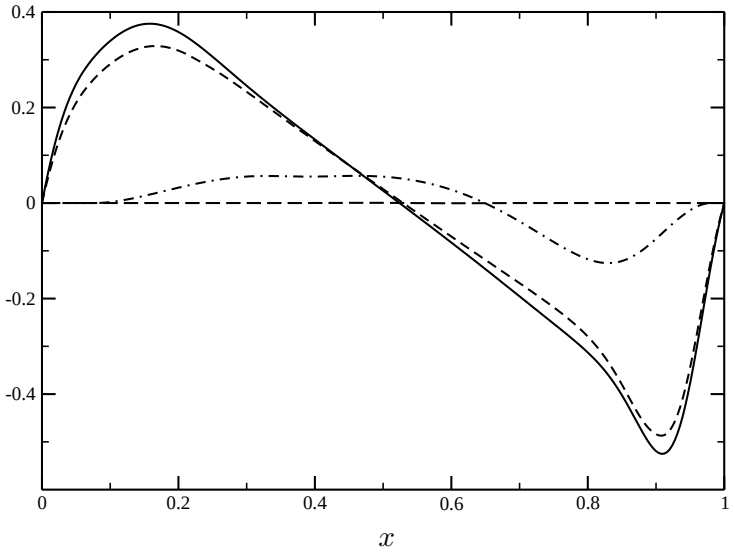

FIGURE 3. Vertical velocity profiles along the centerline $y = 0.5$ for stationnary solutions at $\mathfrak{Re} = 10^3$ and for $\mathfrak{Bi} = 0$ (——), $\mathfrak{Bi} = 1$ (- - -), $\mathfrak{Bi} = 10$ (·-·-) and $\mathfrak{Bi} = 100$ (– – –).

		$x_{\min}$	$\min_x u$	$x_{\min}$	$\min_x v$	$x_{\max}$	$\max_x v$
$\mathfrak{Bi} = 0$	256×256	0.17383	−0.38700	0.90820	−0.52514	0.16211	0.37533
	512×512	0.17188	−0.38817	0.90918	−0.52661	0.15723	0.37658
	1024×1024	0.17139	−0.38847	0.90967	−0.52694	0.15771	0.37685
	Botella and Peyret [4]	0.1717	−0.3886	0.9092	−0.5271	0.1578	0.3769
$\mathfrak{Bi} = 1$	256×256	0.17773	−0.34533	0.90820	−0.48717	0.16211	0.32857
	Vola et al. [26]	0.175	−0.3438	0.9	−0.482	0.1625	0.3286
$\mathfrak{Bi} = 10$	256×256	0.50586	−0.11533	0.83008	−0.12577	0.33008	0.05662
	512×512	0.50488	−0.11628	0.83105	−0.12764	0.32715	0.05714
	Vola et al. [26]	0.5	−0.1156	0.825	−0.1258	0.3375	0.0572
$\mathfrak{Bi} = 100$	256×256	0.58789	−0.0775	0.60742	−0.000438	0.47070	0.000432
	512×512	0.59082	−0.0777	0.60254	−0.000325	0.47754	0.000321
	1024×1024	0.59131	−0.0777	0.60107	−0.000301	0.4790	0.000297
	Vola et al. [26]	0.6	−0.0762	0.6125	−0.0002	0.4625	0.00017

TABLE 1. Values of the velocity extrema along centerlines $x = 0.5$ and $y = 0.5$ for stationary solutions at $\mathfrak{Re} = 10^3$ and for $\mathfrak{Bi}$ in the range $[0, 100]$.

stationary : the discrete time derivatives of the velocity components at $t = 1$ are of the order of 10^{-1} in the L^∞-norm. Let us denote by $\mathbf{u}_{\text{ref}}$ the solution computed on the grid with 2048^2 mesh points and by $\mathbf{u}_h$ the solutions corresponding to coarser grids with mesh size h. We have estimated the numerical error of our scheme by computing the L^2-norm of the difference of $\mathbf{u}_h$

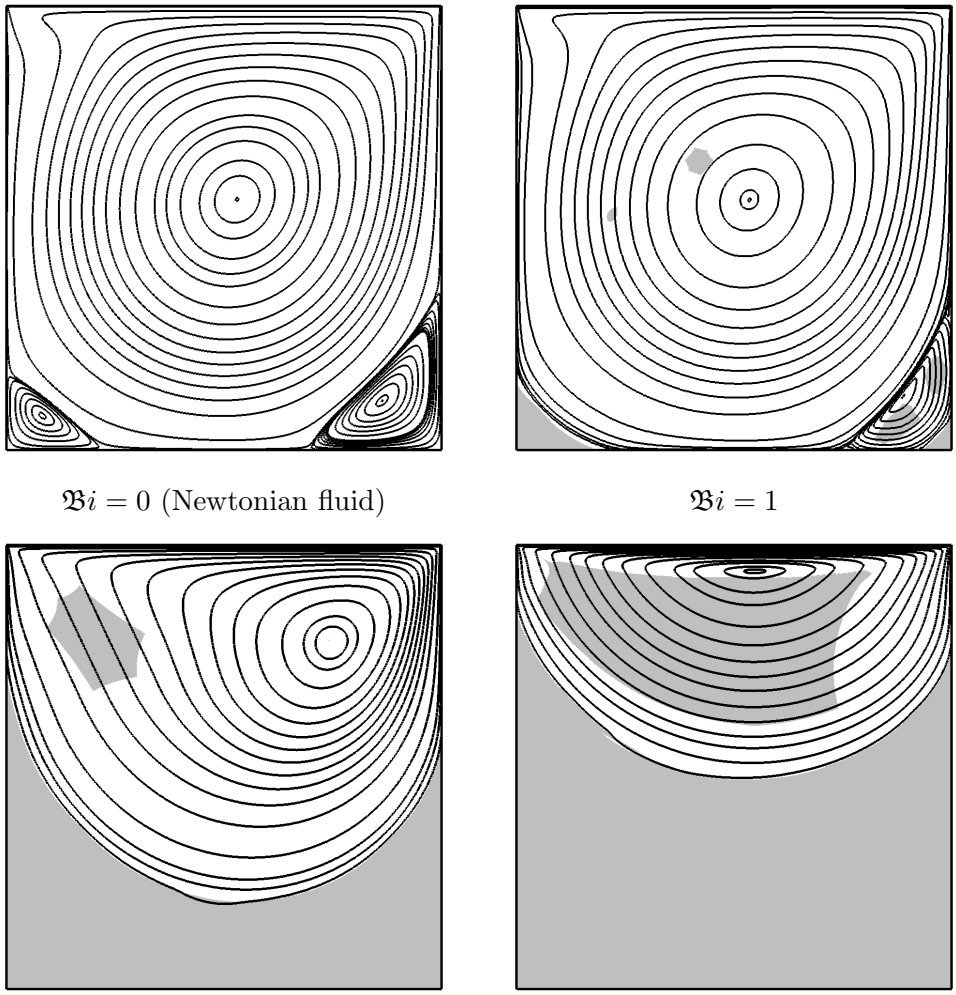

FIGURE 4. Streamlines and rigid zones for flows at $\mathfrak{R}e = 10^3$ and for various Bingham numbers $\mathfrak{B}i$. The spatial resolution is 256^2 for $\mathfrak{B}i = 0$ and $\mathfrak{B}i = 1$, 512^2 for $\mathfrak{B}i = 10$ and 1024^2 for $\mathfrak{B}i = 100$.

with $\mathbf{u}_{\text{ref}}$ at time $t = 1$. The values are plotted on Figure 5 and logarithmic scales are used in order to highlight the convergence rate which is found to be 2 (the slope of the solid line is 2). For this configuration, we therefore obtain a global second-order convergence rate.

4.4. **Finite stopping times.** As it is well known, in the absence of an energy source term, due for instance to the presence of an external volume force and/or nonzero Dirichlet boundary conditions, the solutions of the incompressible Navier-Stokes equations for Newtonian fluids decay exponentially in time. The decay rate depends on the Reynolds number. Dealing with viscoplastic media the flow motion stops in finite time. In order to demonstrate the ability of our numerical procedure to reproduce this important behavior of Bingham flows, we have

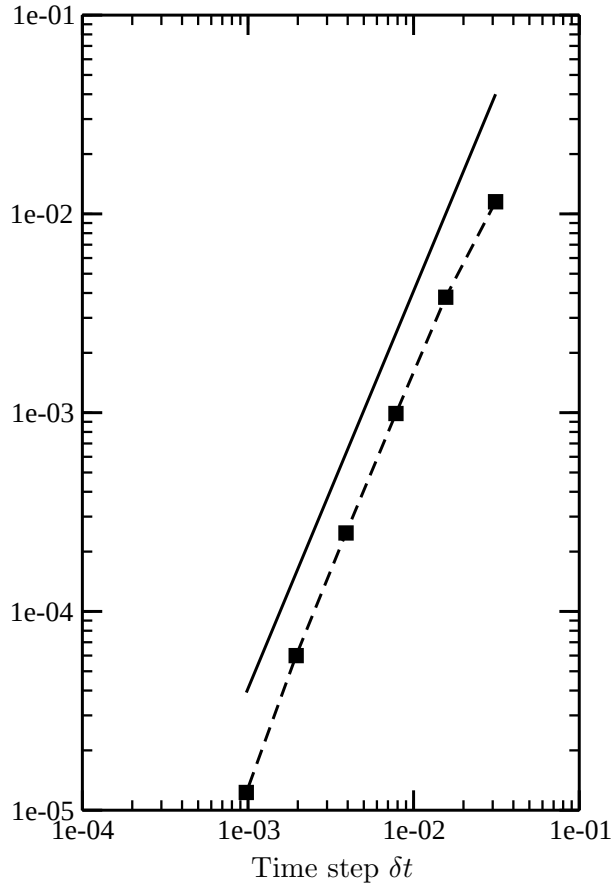

FIGURE 5. Error $\|\mathbf{u}_h - \mathbf{u}_{\text{ref}}\|_2$ at time $t = 1$ plotted as a function of the time step δt which is equal to the mesh size h. Values of h are $1/1024$, $1/512$, $1/128, \ldots, 1/32$. The slope of the solid line is equal to 2.

performed several numerical simulations at $\mathfrak{Re} = 10^3$ in a lid-driven cavity and for various Bingham numbers, namely $\mathfrak{Bi} = 1$, 2.5, 5 and 7.5. The spatial resolution was set to $1/256$ and the time step to 10^{-3}. Starting from rest, the numerical simulations are advanced in time until a steady state is reached. Then, at a stopping time t_{stop}, the energy brought into the system from the upper boundary is stopped, namely : $\mathbf{u}_b(x, 1, t)$ is set to zero for all $t \geq t_{\text{stop}}$. As steady states are reached faster for larger Bingham numbers, we have chosen different values for t_{stop}, namely $t_{\text{stop}} = 40$, 35, 30, 25 for the respective Bingham number $\mathfrak{Bi} = 1$, 2.5, 5, 7.5. On Figure 6, the time evolution of the kinetic energy, defined as

$$K(t) = \frac{1}{2} \int_\Omega \|\mathbf{u}(\mathbf{x}, t)\|^2 \, d\mathbf{x},$$

for these simulations is plotted. For all Bingham numbers used the medium stops in a finite time. The decay of the kinetic energy during the transient period depends on $\mathfrak{Bi}$. As it is expected, the motion stops faster when the Bingham number is larger. These results are qualitatively similar

to those re , that is $\mathfrak{Re} = 1$.

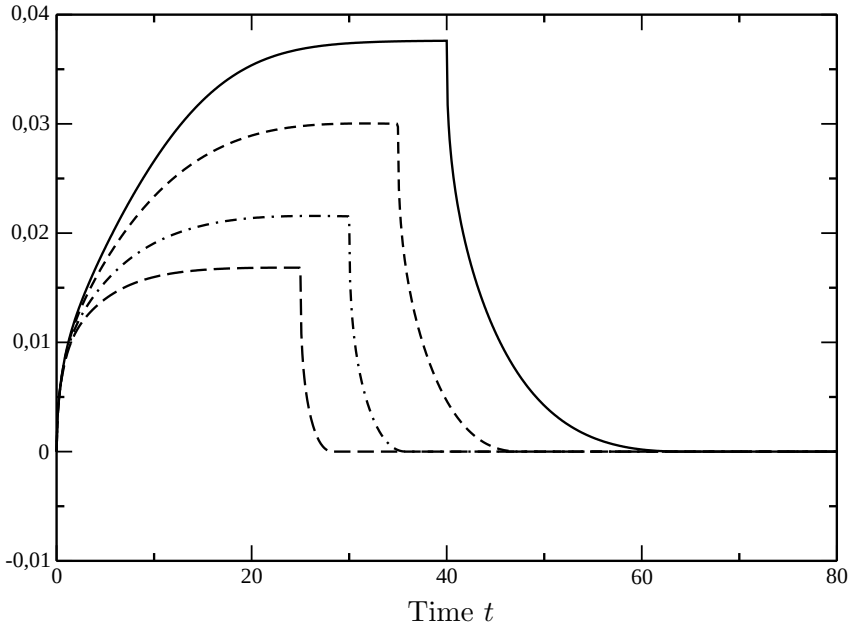

FIGURE 6. Time evolution of the kinetic energy for $\mathfrak{Bi} = 1$ (——), $\mathfrak{Bi} = 2.5$ (- - -), $\mathfrak{Bi} = 5$ (-·-·-) and $\mathfrak{Bi} = 7.5$ (— — —). The stopping time $t_{\text{stop}} \in [25, 40]$ depends on $\mathfrak{Bi}$. The spatial resolution is 256^2.

5. Concluding remarks

A new numerical scheme has been proposed for the time discretization of a system of equations modelling the isothermal and unsteady flow of an incompressible viscoplastic Bingham medium. The non-differentiable definition of the stress tensor is rewritten by introducing a projection operator. The flow is therefore subject to two constraints: the classical one due to the incompressiblity assumption and the second one related to the yield stress tensor. The time discretization is based on a first-order projection scheme, in its incremental version. The plastic (yield) stress tensor is treated implicitely in the prediction step of the projection scheme and is computed with the help of a fixed point algorithm, which is shown to converge geometrically. This is a key feature of the proposed scheme ensuring its numerical efficiency, in terms of consumed computational time.

The first part of the paper is devoted to stability and error analyses of the numerical scheme which is shown to be first-order in time. In a second part, several numerical simulations are performed. The scheme is assessed against previous plubished benchmark results for both Newtonian and Bingham flows in a lid-driven cavity at Reynolds number 10^3 and for various Bingham numbers in the range 1 up to 100. The effect of the mesh resolution on the computed solutions is investigated. For large values of the Bingham number, we observe that the computational grid has to be fine enough in order to properly compute both the fluid and rigid zones characterizing Bingham viscoplastic flows. Also, the proposed numerical scheme is shown to be able to

reproduce the cessation in finite time of a viscoplastic medium in the absence of energy source terms in the equations.

While the proposed numerical scheme applies to a time dependent problem, only convergence to steady state solutions are presented in this paper. Non-stationnary flows in lid-driven cavity exist at much larger values of the Reynolds number, of the order of 100 000 for a Newtonian fluid, and consequently the number of grid points has to be enlarged accordingly. Such numerical simulations are feasible but are out of the scope of this paper and will be presented elsewhere. In order to further demonstrate the efficiency of the bi-projection method proposed and analyzed in this paper, another challenging future work would be to apply the numerical scheme to the numerical simulation of three-dimensional flows. Again, this is postponed to future publications.

Acknowledgements

This research was partially supported by the French Government Laboratory of Excellence initiative n°ANR-10-LABX-0006, the Région Auvergne and the European Regional Development Fund.This is Laboratory of Excellence ClerVolc contribution number 132. The numerical simulations have been performed on a DELL cluster with 32 processors Xeon E2650v2 (8 cores), 1 To of total memory and an infiniband (FDR 56Gb/s) connecting network.

References

[1] S. Balay, S. Abhyankar, M. F. Adams, J. Brown, P. Brune, K. Buschelman, V. Eijkhout, W. D. Gropp, D. Kaushik, M. G. Knepley, L. Curfman McInnes, K. Rupp, B. F. Smith and H. Zhang, *PETSc Web page*, http://www.mcs.anl.gov/petsc, 2014.

[2] S. Balay, S. Abhyankar, M. F. Adams, J. Brown, P. Brune, K. Buschelman, V. Eijkhout, W. D. Gropp, D. Kaushik, M. G. Knepley, L. Curfman McInnes, K. Rupp, B. F. Smith and H. Zhang, *PETSc Users Manual*, Argonne National Laboratory, ANL-95/11 - Revision 3.5, 2014.

[3] M. Bercovier and M. Engelman. A finite element method for incrompessible non-Newtonian flows. *J. Comp. Phys.* **36**, 313-326.

[4] O. Botella and R. Peyret, Benchmark spectral results on the lid-driven cavity flow, *Comp. Fluids* **27** (4), 421–433, 1998.

[5] M. Chatzimina, G.C. Georgiou, I. Argyropaidas, E. Mitsoulis and R.R. Huilgol, Cessation of Couette and Poiseuille flows of a Bingham plastic and finite stopping times, *J. Non-Newtonian Fluid Mech.*, **129**, 117-127, 2005.

[6] E.J. Dean, R. Glowinski, Operator-splitting methods for the simulation of Bingham visco-plastic flow, *Chin. Ann. Math.*, B**23**, 187-204, 2002.

[7] E.J. Dean, R. Glowinski and G. Guidoboni, On the numerical simulation of Bingham viscoplastic flow: old and new results. *J. Non-Newtonian Fluid Mech.*, **142**, 36–62, 2007.

[8] J.I. Diaz, R. Glowinski, G. Guidoboni and T. Kim, Qualitative properties and approximation of solutions of Bingham flows: on the stabilization for large time and the geometry of the support. *Revista de la Real Academia de Ciencias, serie A: Mathematicas*, **104** (1), 2010.

[9] G. Duvaut and J.- L. Lions, Les Inéquations en Mécanique et en Physique. *Dunod*, 1972.

[10] M. Fortin and R. Glowinski, Augmented Lagrangian Methods : Applications to the Numerical Solutions of Boundary-Value Problems, *North-Holland*, Amsterdam, 1983.

[11] R. Glowinski, J.L. Lions and Tremolieres, Numerical Analysis of Variational Inequalities, *North-Holland*, Amsterdam, 1981.

[12] J.-L. Guermond, P. Minev and J. Shen, An Overview of Projection methods for incompressible flows. *Comp. Meth. Appl. Mech. Engng.*, **195**, 6011-6045, 2006.

[13] F.H. Harlow and J.E. Welch, Numerical calculation of time-dependent viscous incompressible flow of fluid with free surface. *Phys. Fluids*, **12**(8), 2182–2189, 1965.

[14] E. Mitsoulis, Flows of viscoplastic materials: models and computations, *Rehology Reviews*, 135-178, 2007.

[15] E. Mitsoulis and Th. Zisis, Flow of Bingham plastics in a lid-driven square cavity, *J. Non-Newtownian Fluid Mech.* **101**, 173-180, 2001.
[16] L. Muravleva, Uzawa-like methods for numerical modeling of unsteady viscoplastic Bingham medium flows, *Applied Numerical Mathematics*, http://dx.doi.org/10.1016/j.apnum.2014.06.001, 2014.
[17] L.V. Muravleva and E.A. Muravleva, Uzawa method on semi-staggered grids for unsteady Bingham media flows. *Russ. J. Numer. Math. Modelling*, **24**(6), 543-563, 2009.
[18] E.A. Muravleva and M.A. Olshanskii, Two finite-difference schemes for calculation of Bingham fluid flows in a cavity. *Russ. J. Numer. Anal. Math. Modelling* **23**(6), 615-634, 2008.
[19] M.A. Olshanskii, Analysis of semi-staggered finite-difference mehod with application to Bingham flows. *Comp. Meth. Appl. Mech. Engng.*, **198**, 975-985, 2009.
[20] T.C. Papanastasiou, Flows of materials with yield. *J. Rheol.* **31**(5), 385-404, 1987.
[21] N. Roquet and P. Saramito, An adaptive finite element method for Bingham fluid flows around a cylinder. *Comput. Methods Appl. Mech. Engrg.* **192**, 3317-3341, 2003.
[22] F.J. Sanchez, Application of a first-order operator splitting method to Bingham fluid flow simulation, *Comput. Math. Appl.*, **36**(3), 71-86, 1998.
[23] J. Shen, On error estimates of the projection methods for the Navier-Stokes equations: first-order schemes. *SIAM J. Numer. Anal.*, **29**, 55-77, 1992.
[24] J. Shen, Remarks on pressure error estimates of the projection methods, *Numer. Math.*, **67**, 513-520, 1994.
[25] R. Temam, Navier-Stokes Equations. Theory and Numerical Analysis. *North-Holland, Amsterdam*, 1984.
[26] D. Vola, L. Boscardin and J.C. Latché, Laminar unsteady flows of Bingham fluids: a numerical strategy and some benchmark results. *J. Comput. Phys.*, **187**, 441-456, 2003.
[27] Y. Zhang, Error estimates for the numerical approximation of time-dependent flow of Bingham fluid in cylindrical pipes by the regularization method, *Numer. Math.* **96**(1), 153-184, 2003.

Laboratoire de Mathématiques UMR 6620, Université Blaise Pascal, Campus des Cézeaux - B.P. 80026, 63171 Aubière cedex, France

E-mail address: Laurent.Chupin@math.univ-bpclermont.fr; Thierry.Dubois@math.univ-bpclermont.fr